The Gaia reference frame amid quasar variability and proper motion patterns in the data

Bachchan, Rajesh Kumar

2015

The Gaia reference frame amid quasar variability and proper motion patterns in the data

Rajesh Kumar Bachchan

Lund Observatory
Lund University

Thesis for the degree of Licentiate of Philosophy

2015

2015-LIC14

Thesis for the degree of Licentiate of Philosophy
Supervisors: David Hobbs and Lennart Lindegren
November 2015

Lund Observatory
Box 43
SE-221 00 Lund
Sweden

The Gaia reference frame amid quasar variability and proper motion patterns in the data

By

Rajesh Kumar Bachchan

Supervisors:
Dr. David Hobbs
Prof. Lennart Lindegren

November 11, 2015

This thesis is submitted as a requirement of Licentiate Degree
in Astronomy & Astrophysics
to the
Department of Astronomy & Theoretical Physics
Lund University, Sweden

ACKNOWLEDGEMENTS

It was a great opportunity to work with very cooperative supervisors Dr. David Hobbs and Prof. Lennart Lindegren. During this work, their support, helpfulness and constant encouragement kept me motivated in my research work. They provided invaluable interest and guidance during the course of the work and constantly went through the whole draft word by word. I have not only learned various software skills but also got important suggestions regarding scientific writing and other related matters. I am very grateful for all their input.

I express sincere thanks to the Swedish National Space Board for providing the scholarship to carry out the work. Finally, I would like to express my sincere thanks to all the faculty members, staff and friends at Lund Observatory for making a very friendly environment during my stay.

Rajesh Kumar Bachchan
November 11, 2015

Contents

ABBREVIATIONS

A&A	Astronomy and Astrophysics
AGIS	Astrometric Global Iterative Solution
AJ	The Astronomical Journal
ApJ	The Astrophysical Journal
AP&SS	Astrophysics and Space Science
ASP	Astronomical Society of the Pacific
ARA&A	Annual Review of Astronomy and Astrophysics
CCD	Charged Coupled Device
CDS	Centre de Données astronomiques de Strasbourg
COBE	Cosmic Background Explorer
CMB(R)	Cosmic Microwave Background (Radiation)
CoMRS	Centre of Mass Reference System
Dec	Declination
DPAC	Data Processing and Analysis Consortium
ECS	Equatorial Coordinate System
ESA	European Space Agency
FRW	Friedmann-Robertson-Walker
GCS	Galactic Coordinate System
GTR	General Theory of Relativity
GUMS	Gaia Universe Model Snapshot
IAU	International Astronomical Union
ICRF	International Celestial Reference Frame
ICRS	International Celestial Reference System
IGQL	Initial Gaia Quasar List
ly	Light Year
LMC	Large Magellanic Cloud
LOS	Line Of Sight
LTB	Lemaitre-Tolman-Bondi
MOND	Modified Newtonian Dynamics
Mpc	Megaparsec
NASA	National Aeronautics and Space Administrations
NCP	North Celestial Pole
NED	NASA Extragalactic Database
NGC	New General Catalogue (of nebulae and clusters of stars)
NGP	North Galactic Pole
PPN	Parametrized Post Newtonian
SCP	South Celestial Pole
SCS	Supergalactic Coordinate System
SRS	Scanning Reference System
pc	parsec
RA	Right Ascension
RV	Radial Velocity
SMC	Small Magellanic Cloud

UGC	Uppsala General Catalogue (of galaxies)
VLBI	Very Long Baseline Interferometry
VLBA	Very Long Baseline Array
VCS	VLBA Calibrator Survey
Web	Website

ABSTRACT

The astrometric satellite Gaia was launched in December, 2013. It will observe nearly one billion stars in the Milky Way and beyond along with many extragalactic objects such as quasars and galaxies. The analysis of quasar data will provide the optical counterpart of the International Celestial Reference Frame (ICRF). Also, the analysis of data for stars in our Galaxy provide a revolution in our understanding of Galactic dynamics, formation and evolution.

The ICRF with its origin at the barycentre of the Solar System is based on distant quasars assumed to be static on the celestial sphere. With the expectation of a very large number of quasars from Gaia measurements, we study the effect of photocentric variability of quasars on the optical stability of the reference frame. The photocentric variability is modelled using a Markov chain model. In addition, there are many astrophysical and cosmological sources of proper motion. We review these effects of which the most significant are the secular aberration drift due to the acceleration of the Solar System, and the motion of the Sun relative to the Cosmic Microwave Background (CMB). Based on simulated data, the reference frame along with the Solar System acceleration is determined using an algorithm developed for the Gaia mission.

We conclude that the photocentric variability of quasars does not have a very significant impact on the recovery of the reference frame. However, we notice a correlation between the frame parameters and the acceleration due to the inhomogeneous all-sky distribution of quasars. We also try to astrometrically determine our velocity relative to the CMB based on a cosmological model. Alternatively, if we assume that our velocity relative to the CMB is known from other missions, such as Planck, we can in principle measure the Hubble constant by astrometric means. This measurement is however very difficult and will require accurate centroiding on extended objects.

Chapter 1

Introduction

The curiosity of people about stars and other objects in the sky led to the invention of astronomical telescopes in the 17^{th} century. Subsequently, many new discoveries like asteroids, galaxies, quasars, exoplanets etc occurred. By gathering the data on positions, parallaxes and motions of stars, great insight into the dynamics and distance scales within our Galaxy can be achieved. However, observing objects through the Earth's atmosphere distorts the images as seen from the ground. This problem in particular led to the development of space based telescopes equipped with the necessary instruments to record and send images and measurements back to the Earth for further processing. Prime examples of this are the Hubble Space Telescope and the Hipparcos satellite. There are also many benefits of space telescopes over ground based telescopes, e.g. visualisation of the whole sky at the same time, elimination of mechanical deformation of the instrument thanks to weightlessness, thermally and mechanically stable environment etc (van Altena, 2013).

The study of the geometrical relationships between objects in the sky and their apparent and true motions is called astrometry. The basic idea behind distance measurement of a star is stellar parallax. Suppose we observe a star at S (Fig. 1.1) from the position E against the distant far away stars, and

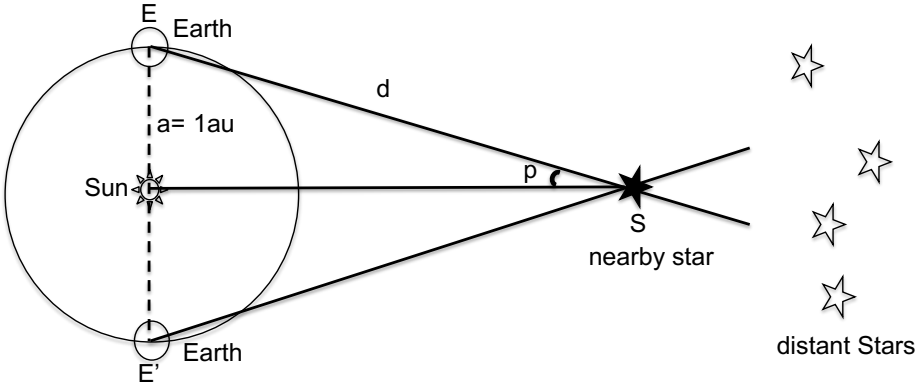

Figure 1.1: Stellar parallax

again after six months from position E'. In this time interval, the star appears to shift in its position.

From the geometry of the figure we have, in the small angle approximation,

$$p^{\text{rad}} = \frac{a}{d}$$

This is called the annual parallax of the star. Expressed in *arcsecond*, we can write

$$p'' = \frac{a}{d} \times \frac{180}{\pi} \times 3600 \quad \text{or} \quad d \simeq \frac{206265a}{p''}$$

If we take $206265a$ as the unit of distance then

$$d \simeq \frac{1}{p''}$$

The unit of distance is called a *parsec* (pc). For $p = 1$, $d = 1$. Thus, 1 *pc* is the distance at which the radius (a) of Earth's orbit around the Sun subtends an angle of $1''$:

$$1 \text{ pc} = 206265a = 3.26 \text{ ly} = 3.082 \times 10^{16} \text{ m}$$

Knowing the distance to a star, we can deduce its absolute magnitude M (the absolute magnitude is the magnitude of an object if it is observed at a distance of 10 pc):

$$M = m - 5 \log_{10} d + 5 \tag{1.1}$$

where m is apparent magnitude and d is the distance in *parsec*. Extinction is ignored in this equation.

Using the method of parallax, distances up to a few tens of kiloparsec will be measured to some degree of accuracy. To measure even larger distances we have to use objects like cepheid variables or RR Lyrae variables and in the extreme case Type Ia supernovae. Such objects whose absolute magnitude is constant or can be derived from observed quantities (such as the period of a cepheid variable) are called standard candles. Their distances can then be calculated using the relation (1.1).

In addition to parallax, another important quantity is 'proper motion'. A star at a certain distance from us appears to move tangentially across the sky. So, from the initial line of sight, in one year, the star appears to move through an angle μ. This angle is termed as 'proper motion'. If a star at a distance d has tangential velocity v_t then

$$\mu = \frac{v_t}{d} \tag{1.2}$$

In this work, we have made a study of various phenomena that can give rise to proper motion patterns in the observation of quasars and galaxies and we have considered the reference frame (in-)stability that could result from such motions. Next, we shall briefly introduce the astrometric satellite Gaia as this work uses simulated data for this mission to assess how well the real mission will perform. For the details of how Gaia works and the many algorithms involved in the Gaia data processing, see Lindegren et al. (2012).

1.1 The Gaia satellite

The Gaia satellite developed by the European Space Agency (ESA) was launched in December 2013 from French Guiana by Arianespace. Gaia is a successor mission to an earlier astrometric satellite called Hipparcos, which was launched in 1989. The accuracy of Hipparcos was in milli-arc-second (10^{-3} arc seconds) range. A catalogue was created with the positions, parallaxes and proper motions of ~120000 stars. The accuracy of Gaia will be of the order of 10 μas for bright stars (V~10) degrading to around 25 μas at V = 15, and to around 0.3 mas at V = 20 (Perryman, 2014). Here, V $\equiv m_V$ stands for V-band apparent magnitude. By convention, the brighter an object is, the smaller is its magnitude.

Gaia will be placed in a Lissajous-type orbit, around the second Lagrangian point ($L2$) of the Sun-Earth system which is located at about 1.5 million kilometers from the Earth. This L2 point represents a location where the combined gravitational pull of the Earth and the Sun exactly balance the centrifugal force in the one year satellite orbit. The Lissajous orbit avoids the Earth's shadow and provides a very stable thermal environment. Gaia will remain in the orbit for at least five years, spinning continuously around its axis with a period of six hours. It sends to the Earth terabytes of data, the processing of which may take a further three years after the end of the mission. To process the data, software has been developed by the Data Processing and Analysis Consortium (DPAC). There will be several early data releases; however, the final data will be in the public domain around 2022 assuming the mission is not extended.

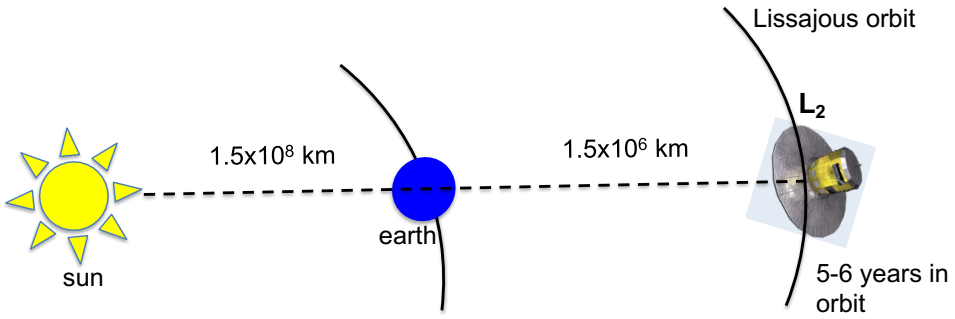

Figure 1.2: The orbit of Gaia.

The Gaia satellite consists of two telescopes (line of sights) separated by an angle of 106.5° and each having a focal length of 35 m with a common focal plane. Each telescope covers 0.45 deg^2 and has six mirrors M1-M6. There is a beam combiner after the third mirror which combines the images from the two telescopes (web[3]). The full optical system with a diameter of 3 m is shown in Fig. 1.3. On the focal plane lies five groups of CCDs as shown in Fig. 1.4. In total there are 106 CCDs each having a pixel size of 10μm × 30μm (web[4]). Below, we mention in brief the functions of each group of CCDs.

1. Basic Angle Monitor (BAM): It tracks any variation in the basic angle of 106.5° between two line of sights using a laser interferometer.

2. Sky Mapper (SM): This makes the first detection of the stars from each line of sight (LOS)

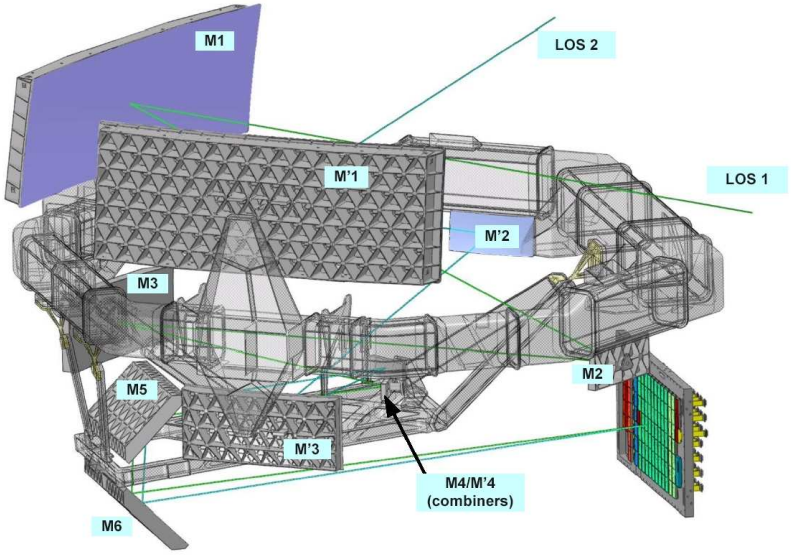

Figure 1.3: Gaia Payload (Image: Astrium (web[4]))

one for each of the two CCD strip. If an object appears on SM-1 then it is from LOS-1, similarly for LOS-2.

3. Astrometric Field (AF): Theses are the main CCDs for astrometry and the main astrometric measurements are made here.
4. Photometers (BP and RP): The next two strips are the blue and the red photometers. These operate in the 330-660 nm and 650-1000 nm range for BP and RP respectively, and provide photometric measurements using dispersive prisms.
5. Radial Velocity Spectrograph (RVS): This set of CCDs which operate in the near infrared region 847-874 nm provide the radial velocity measurements of stars down to 16th magnitude.

1.2 Gaia Astrometric Processing

The basic idea of the Gaia data analysis is the minimisation of the following (Lindegren, 2012):

$$\min_{(\mathbf{s},\mathbf{n})} \|\mathbf{f}^{\text{obs}} - \mathbf{f}(\mathbf{s},\mathbf{n})^{\text{calc}}\| \tag{1.3}$$

Here, $\mathbf{s}$ is a vector of unknowns which describe the barycentric motions of the stars. $\mathbf{n}$ is a set of "nuisance parameters" namely, attitude $\mathbf{a}$, geometric calibration $\mathbf{c}$ and global parameters $\mathbf{g}$. $\mathbf{f}(\mathbf{s},\mathbf{n})^{\text{calc}}$ represents the expected detector coordinates. The observables $\mathbf{f}^{\text{obs}}$ are the measured positions of the stars on the CCDs at a given time.

The final output of Gaia will be six astrometric parameters $\mathbf{s}_i(\alpha_i, \delta_i, \varpi_i, \mu_{\alpha*i}, \mu_{\delta i}, \mu_{ri})$ for each star (i) in the ICRS reference system (Sect. 1.3.2). However, μ_r cannot be measured accurately from the astrometric observations. For most stars, it is measured separately by RVS using the Doppler shift or is assumed to be zero. When a star passes over the focal plane (or CCDs) we measure the time

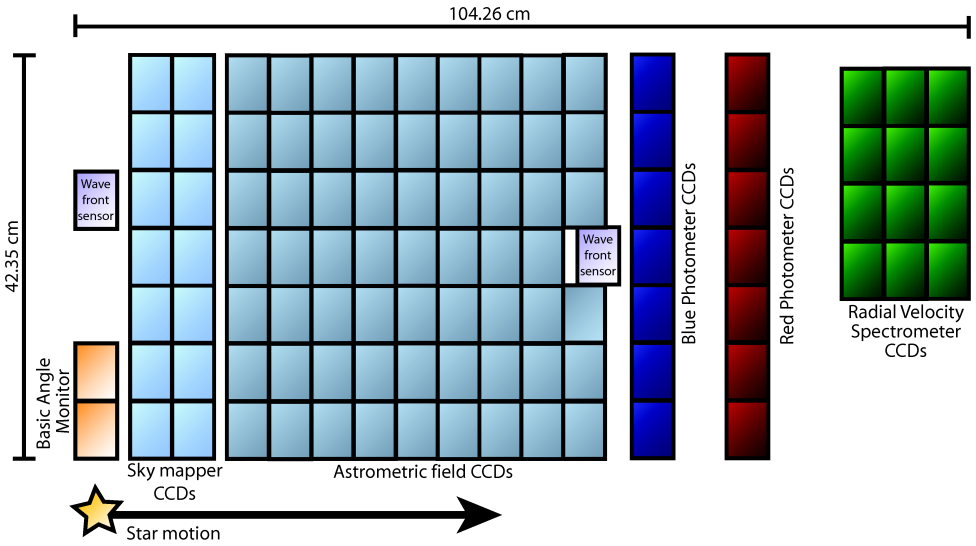

Figure 1.4: Arrangement of CCD in Gaia (Image: Astrium (web[3])). In the Gaia DPAC terminology, columns are referred to as strips.

at which it passes a reference line on the CCDs which is used to define its coordinates. From the CCD coordinates, we transform to the Scanning Reference System (SRS) (instrument axes) with origin at the centre of mass of Gaia and axes fixed with the instrument so that it rotates with the satellite. Basically, the axes are defined based on the two fields of view of the satellite and is not aligned with the non-rotating ICRS. From SRS we have to map to the Centre of Mass Reference System (CoMRS) which is kinematically non-rotating and aligned with the ICRS and the centre is the centre of mass of the satellite. The orientation of the spacecraft in the CoMRS relative to the SRS is called the Gaia attitude (Lindegren, 2012). By using the attitude, we can transform from the SRS to the CoMRS. Finally from the CoMRS to the ICRS is a another coordinate transformation. This process can also be pictorially represented as in Fig. 1.5.

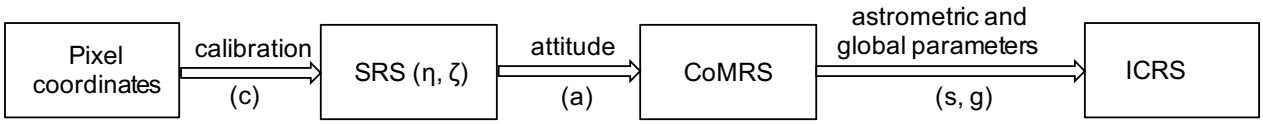

Figure 1.5: Gaia Astrometric Processing

Assuming that all the sources move with uniform space velocity, their coordinates at time t_* in BCRS are given by (Lindegren, 2012)

$$\mathbf{b}_i(t_*) = \mathbf{b}_i(t_{\rm ep}) + (t_* - t_{\rm ep})\mathbf{v}_i \tag{1.4}$$

where $t_{\rm ep}$ is an arbitrary reference epoch, $\mathbf{b}_i(t_{\rm ep})$ and $\mathbf{v}_i$ define the six kinematic parameters for the motion of the source. While Eq. (1.4) fully describes the astrometric model, the uniform astrometric parameters are a transformation of the kinematic parameters which are more suitable for astrometric

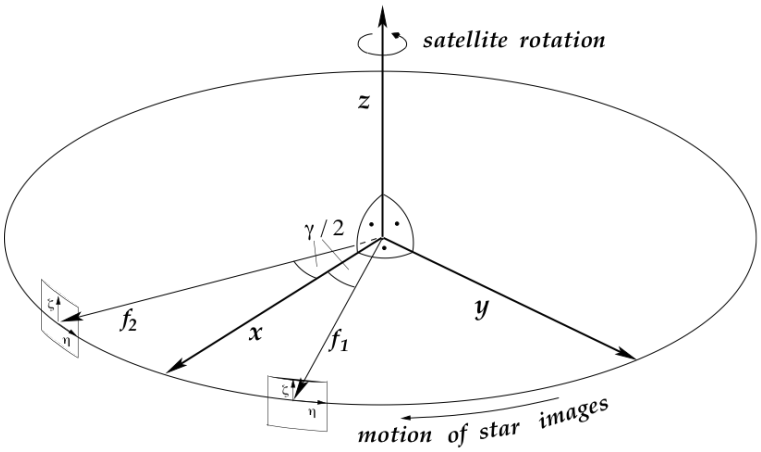

Figure 1.6: The two field of view f_1 and f_2 in the Gaia satellite at an angle of 106.5° along with the SRS coordinates $(\eta,\ \zeta)$ (Bastian, 2007).

measurements. Let t_* below be the time at which a source emits light and t be the time at which Gaia sees it. Then the coordinate direction to the source at time t is given by the reduction of

$$\bar{\mathbf{u}}_i(t) = \left\langle \mathbf{r}_i + (t_B - t_{\rm ep})\left(\mathbf{p}_i\mu_{\alpha*i} + \mathbf{q}_i\mu_{\delta i} + \mathbf{r}_i\mu_{ri}\right) - \frac{\varpi_i \mathbf{b}_G(t)}{a} \right\rangle \tag{1.5}$$

where

$$\begin{aligned}
[\mathbf{p}_i\ \mathbf{q}_i\ \mathbf{r}_i] &= \text{normal triad of the source with respect to ICRS}\\
\mathbf{r}_i &= \text{barycentric coordinate direction to the source at time } t_{\rm ep}\\
\mathbf{b}_G(t) &= \text{barycentric position of Gaia at the time of observation}\\
a &= \text{the astronomical unit}\\
\text{and}\quad t_B &= t + \frac{\mathbf{r}_i'\mathbf{b}_G(t)}{c}
\end{aligned}$$

The transformation from the coordinate direction $\bar{\mathbf{u}}_i(t)$ to the observable direction $\mathbf{u}_i(t)$ is then given by the model described by Klioner (2003) which takes into account the light bending effect and the global parameters such as PPN γ. The full details can be found in the given reference. Here, we just give the basic idea.

At a certain instant of time, the observer sees the source in the direction **s** and **n** is the tangent vector to the light ray. The difference in these two directions is the aberration. **k** is the vector from the source to the observer. So, the step from **n** to **k** is the correction due to gravitational light bending. **l** is the vector from barycentre of the Solar System to the source. The last step is therefore the parallax correction from **k** to **l** i.e.,

$$\mathbf{s} \xrightarrow{\text{aberration}} \mathbf{n} \xrightarrow{\text{grav. light bending}} \mathbf{k} \xrightarrow{\text{parallax}} \mathbf{l}$$

All the vectors are unit vectors. (The unit vector **s** should not be confused with the stellar parameter vector **s** in Eq. (1.3).)

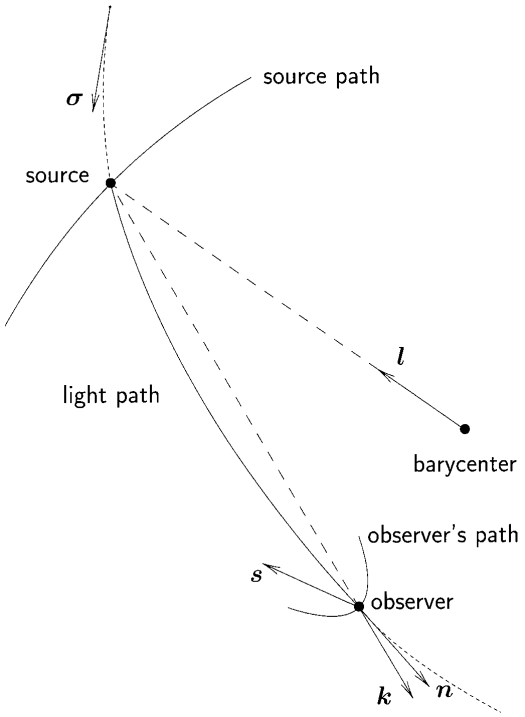

Figure 1.7: Relativity model for position observation (Klioner, 2003)

The objective of Gaia (Robin et al. 2012) is to measure precisely positions, proper motions, parallaxes and velocities of one billion stars (~1%) in our Galaxy, the Milky Way. The measurements of Gaia will provide an accurate picture of the structure and kinematics of the Milky Way from which its composition, formation and evolution may be derived. Moreover, Gaia will also find thousands of asteroids, brown dwarfs and exoplanets of at least Jupiter size outside our Solar System. It will also observe about 500,000 quasars and a large number of galaxies. It will help us to study the dynamics of the Local Group galaxies like Andromeda, Large Magellanic Cloud (LMC), Small Magellanic Cloud (SMC) and others. The study of alignment of angular momentum of galaxies will provide an insight on how galaxies are formed, how they obtain their angular momentum etc. (Hu et al. 2006).

Gaia will also play an important role in fundamental physics, for example testing Einstein's general theory of relativity and any deviations from it owing to the fact that Gaia will determine the light bending term (PPN - γ) to very high precision. In this work, apart from the reference frame and the Galactocentric acceleration, we have investigated a cosmological phenomenon, namely the proper motion of galaxies due to our motion relative to the CMB or alternatively to astrometrically measure the Hubble parameter. This effect is described in detail in Sect. 2.2.

1.3 Coordinate Systems

Quite often in astronomy, we have to deal with different types of coordinate systems depending on the type of object and investigation. For example, for objects in our Galaxy, the Galactic Coordinate System (GCS) or the Equatorial Coordinate System (ECS) is used whereas for very large scale dynamics e.g., cluster, supercluster, the Supergalactic Coordinate System (SCS) is used. Here, we shall give a brief introduction to ECS, GCS and the International Celestial Reference System (ICRS).

1.3.1 Equatorial Coordinate System

In this coordinate system, with the earth as the centre, we draw a celestial sphere as shown in Fig. 1.8. NCP and SCP stands for North Celestial Pole and South Celestial Pole respectively. γ (vernal equinox) is used as the zero point for right ascension (RA or α). This points corresponds to the position of the Sun when it crosses the celestial equator in the ascending direction. The coordinates of an star (S) are then given by (α, δ). RA lies between 0 and 360° i.e., $0 \leq \alpha \leq 360°$. It can also be expressed in (h m s) as 24 hours = 360°. On the celestial equator, $\delta = 0$. At NCP, $\delta = +90°$ and at SCP, $\delta = -90°$.

The ECS, being linked to the rotation of the Earth, is relevant e.g. for pointing a ground based telescope to a given object. However, because the direction of Earth's axis and the vernal equinox are changing due to precession and nutation, ECS is unsuitable for general reference purposes. For this reason, it has been superseded by the ICRS.

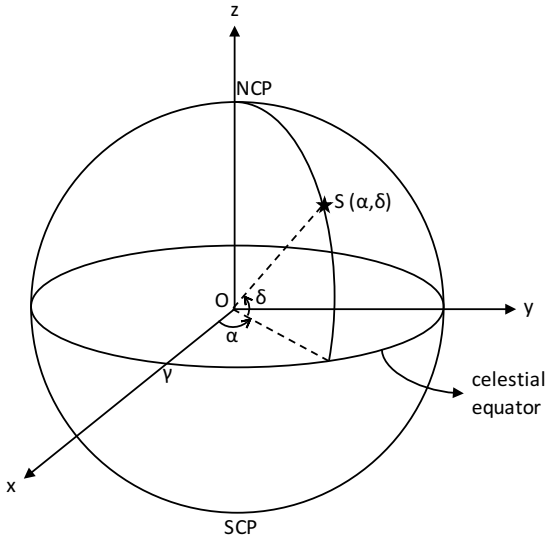

Figure 1.8: Equatorial Coordinate System (Green, 1985)

1.3.2 International Celestial Reference System

The International Celestial Reference System (ICRS) is the reference system officially adopted by the International Astronomical Union (IAU) in 1997. Its origin is at the barycenter of the Solar System and the axes are fixed with respect to space (web[1]). Its practical realisation is based on Very Long Baseline Interferometry (VLBI) observations of extragalactic sources and the corresponding frame is called the International Celestial Reference Frame (ICRF). The origin of RA of the ICRF is defined by adopting the mean RAs of 23 radio sources from catalogues compiled by fixing the RA of the radio source 3C273B to the FK5 value (12h 29m 6.6997s at J2000.0) (Kovalevsky, 2004). The ICRS coordinates are nearly the same as equatorial coordinates. The fundamental plane ($\delta = 0$) and the zero point ($\alpha = 0,\ \delta = 0$) of the ICRF nominally match the Earth's equatorial plane and the direction to the dynamical vernal equinox at the beginning of the year J2000 respectively (Bastian, 2007).

The ICRF1 (adopted in 1998) consists of J2000.0 VLBI coordinates of 608 extragalactic radio sources evenly distributed on the sky of which 212 objects are the defining sources. They define the ICRF axes. The precision of the positions of the ICRF1 reference points and the accuracy in the orientation of its axes are 100 times better than those of the previous IAU official celestial reference frame, the FK5. In ICRF, the definition of the axes of the celestial reference system is not related to the equator or the ecliptic like in FK5; it is totally independent of the Solar System dynamics. The

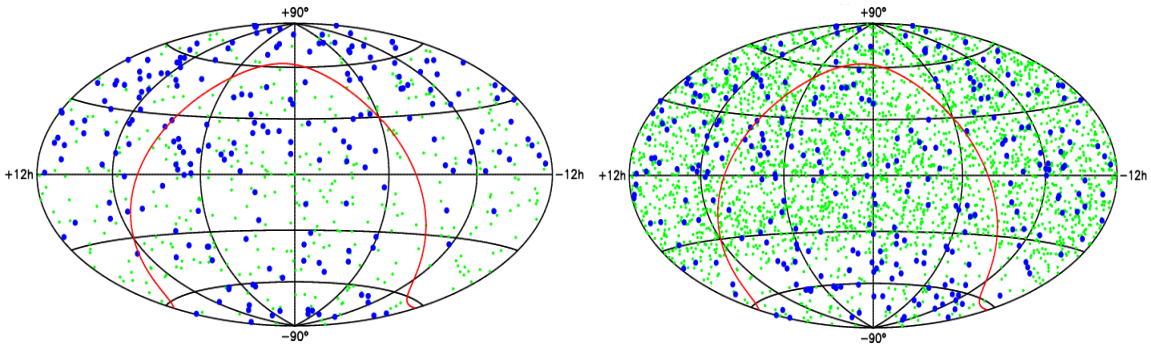

Figure 1.9: (a) ICRF1 (b) ICRF2. The blue dots are for defining sources while green dots are for other sources (Capitaine, 2012).

further refinement of ICRF1 brings ICRF2 (adopted in 2010) consisting of 3414 radio sources of which 295 are the defining sources. Its accuracy is 5-6 times better than that of the ICRF1 and the axes are nearly twice as stable as in ICRF1.

In ICRF2, nearly two-thirds of the sources are from the VLBA Calibrator Survey (VCS) and their coverage is weak south of declination $-30°$ (Fig. 1.9b) because of a lack of observations and the VCS positions are five times worse than ICRF2. Similarly, many sources are not point-like and this induces systematic error. These discrepancies show the need for a next generation of ICRF i.e., ICRF3. It is expected that the necessary radio candidates will be ready by 2018 with an accuracy of 70 μas which, when tied with the Gaia optical frame, will provide a much more accurate reference frame (Jacobs et al. 2014).

1.3.3 Galactic Coordinate System

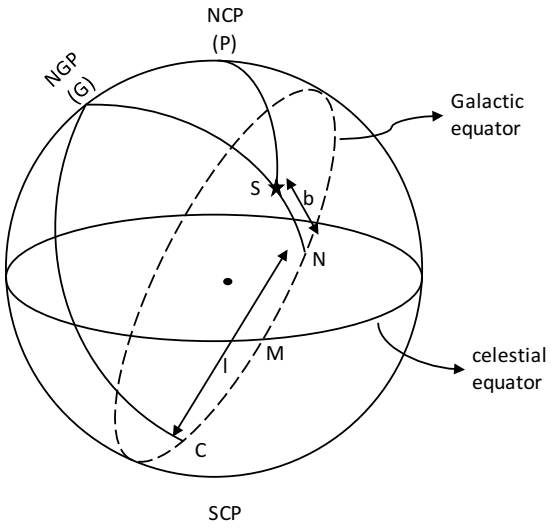

Figure 1.10: Galactic Coordinate System (Green, 1985)

This coordinate system is similar to ECS, except that in this case the equator is the Galactic equator which passes through the plane of Galaxy and the pole is the North Galactic Pole (NGP). Referring to Fig. 1.10, the galactic longitude and the galactic latitude are given by

$$l = CN = CGS \qquad 0 \leq l \leq 360^\circ$$
$$b = NS = 90^\circ - GS \qquad -90^\circ \leq b \leq 90^\circ$$

where C is the direction to Galactic centre. The orientation of GCS relative to ECS is shown in Fig. 1.10 from which we can easily transform from one system to another. For the necessary transformation relations see for example Spherical Astronomy (Green, 1985). It should be noted that the International Astronomical Union (IAU) has not (yet) adopted an official transformation from ICRS to GCS, and that several different versions of GCS are therefore currently in use.

Chapter 2

Sources of Proper Motion Patterns

The study of stellar motions reveals a great deal of information in astrophysics and cosmology. The parameters that are of importance here are positions, parallax and proper motion, denoted by (α, δ), ϖ, $(\mu_{\alpha*}, \mu_\delta)$ respectively. Measuring the positions of objects together with the associated uncertainties gives a clear idea about their locations on the celestial sphere. The study of parallax along with the associated error indicates the distance to the celestial objects. Similarly, the measurement of proper motions also provides an idea of the objects motion on the celestial sphere and how they move relative to each other.

In the context of cosmology, the study of proper motion is also very important. By measuring proper motion along with Galactocentric acceleration, we can check various anisotropic models of the universe. Similarly, it can help us to understand our own motion relative to the CMB background. The measurement of proper motion patterns may provide insight into the existence of gravitational waves and the presence of dark matter via microlensing.

We have tabulated below and also explained in the following subsections several of the proper motion patterns which could potentially be observed using Galactic and extragalactic objects.

Table 2.1: Various physical phenomena that may contribute to proper motion patterns in the observable universe.

Effect	Description	Expected magnitude
Acceleration of the Solar System	Acceleration of the Solar System assumed to be towards the Galactic centre resulting in patterns of proper motion. However, the local group of galaxies and clusters of local supercluster will also contribute to the effect.	~4.3 μas yr^{-1} (independent of distance)
Cosmological proper motion	Instantaneous velocity of the Solar System with respect to the CMB can cause distant extragalactic sources to undergo an apparent systematic proper motion.	1–2 μas yr^{-1} (z~0.01)
Gravitational waves	Primordial gravitational waves produce systematic proper motions over the sky.	Unknown but probably < 1 μas yr^{-1}
Cosmic parallax	A temporal shift of the angular separation of distant sources can be used to detect an anisotropic expansion of the universe and results in a pattern of proper motions.	0.2 μas yr^{-1} (Bianchi) 0.02 μas yr^{-1} (LTB)
Peculiar proper motion	Proper acceleration is the observed transverse acceleration of an object due to the local gravitational field.	Can be 10 μas yr^{-1} for Galactic clusters (z~0.01)
Quasar microlensing	Weak microlensing can induce apparent motions of quasars.	10's of μas yr^{-1} but is extremely rare

2.1 Motion of the Solar System around the Galactic centre

As we know the Sun (or Solar System) is orbiting the Galactic centre with a velocity of ~220 km s^{-1} (Fig. 2.1). This causes an aberration effect of ~2.5′ which changes slowly with time (Bastian, 1995). The result is a proper motion pattern (Fig. 2.2) whose amplitude is calculated as

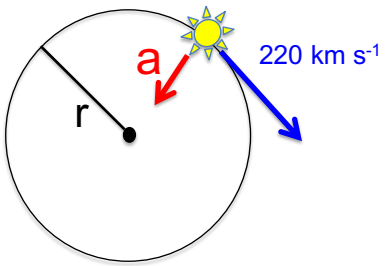

Figure 2.1: Galacto-centric acceleration

$$\mu = \frac{a}{c} = \frac{1}{c}\left(\frac{v^2}{r}\right) = 4.3 \ \mu\text{as yr}^{-1} \tag{2.1}$$

where, $v = 220$ km s^{-1}, $r = 8.0$ kpc and $c = 3 \times 10^8$ m s^{-1}.

Also, the other member galaxies of the local group along with large scale structures in the universe, such as clusters and superclusters, also induce an apparent proper motion pattern by their gravitational attraction. However, the amplitude in these cases is very small ($\ll 1$ μas yr^{-1}).

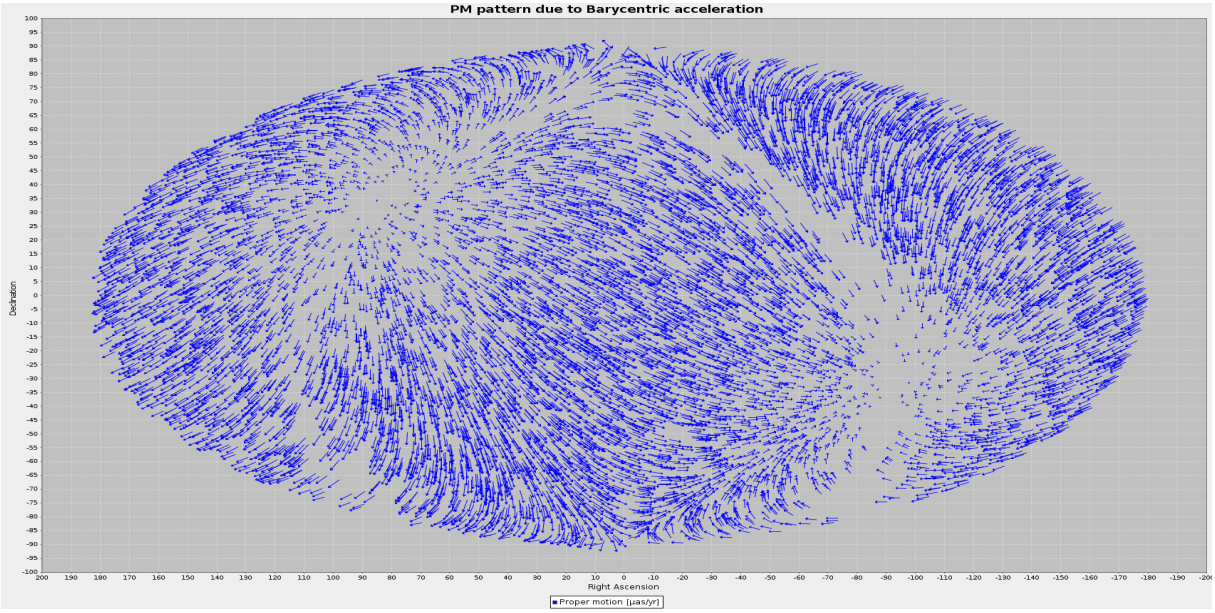

Figure 2.2: Example of the proper motion pattern due to the acceleration of the Solar System, determined in our simulations including quasars and low redshift galaxies. The vectors are anchored to the objects position and their lengths are scaled to match a pattern of 4.3 μas yr^{-1}. Only a small random sample of 10,000 vectors is shown for clarity. The coordinates are in the equatorial system.

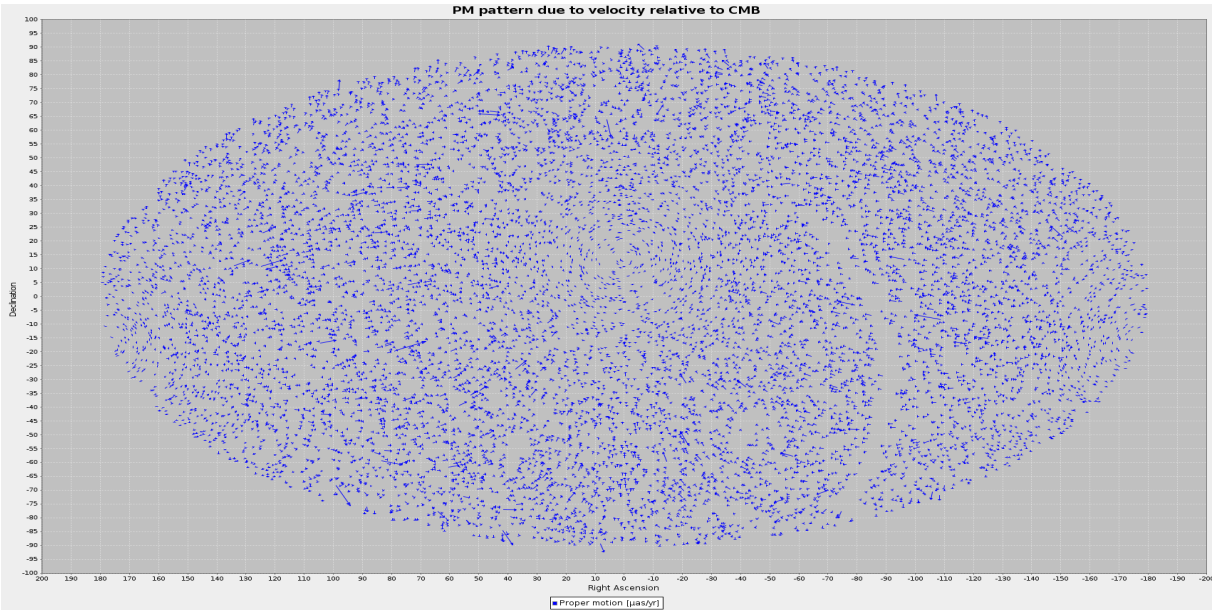

Figure 2.3: Example of the proper motion pattern due to the velocity of the Solar System relative to the CMB, determined in our simulations including only low red shift galaxies. The vectors are anchored to the objects position and their lengths are scaled to match a velocity of 369 km s^{-1}. Only a small random sample of 10,000 vectors are shown for clarity. This pattern is much less distinct than in Fig. 2.3 as only the lowest red shift galaxies have a significant contribution. The coordinates are in the equatorial system.

2.2 Motion of the Sun relative to the Cosmic Microwave Background

Kardashev (1986) pointed out that the primordial electromagnetic background provides a comoving reference frame with respect to which the motion of an object can be measured. The velocity of the Sun relative to the Cosmic Microwave Background (CMB) is 380 ± 30 km s^{-1} in the apex direction $l = 253° \pm 5°$ and latitude $b = 47° \pm 5°$. The result of the COBE satellite gives a value 371 ± 1 km s^{-1} towards $(l,\ b) = (264.14° \pm 0.15°, 48.26° \pm 0.15°)$ (Fixsen, 1996). The result from Planck gives a value of $v = 369 \pm 0.9$ km s^{-1} towards $(l,\ b) = (263.99° \pm 0.14°,\ 48.26° \pm 0.03°)$ (Aghanim, 2014).

This motion will produce a parallactic shift of all extragalactic objects towards the antapex (Fig. 2.3) at an angular rate

$$\mu = \mu_0 \sin\beta \tag{2.2}$$

where $\mu_0 = v/d$ with d given by the transverse comoving distance,

$$d(z) = \frac{c}{H_0} \int_0^z \frac{dz}{\sqrt{\Omega_m(1+z)^3 + \Omega_r(1+z)^4 + \Omega_k(1+z)^2 + \Omega_\Lambda}} \tag{2.3}$$

β is the angle between the source and apex directions, $H_0 = 67.3$ km s^{-1} Mpc^{-1} is the Hubble's constant (Aghanim, 2014) and $\Omega_m,\ \Omega_r,\ \Omega_k,\ \Omega_\Lambda$ are the densities of matter, radiation, curvature and cosmological constant respectively. For most of the cases, we can neglect Ω_r as it is very small and for a flat Universe, we can take $\Omega_k = 0$ and the values of Ω_m and Ω_Λ are 0.3 and 0.7 respectively.

As d increases rapidly (initially linearly) with redshift then the proper motion amplitude must decrease rapidly with redshift. This obviously has implications for rejecting the types of sources used to study this effect.

2.3 Primordial gravitational waves

Pyne et al. (1996) pointed out that when light propagates through gravitational waves it preserves the surface brightness and the total intensity of the source to first order in the wave amplitude. It can also produce oscillations in source position with period compared to that of gravitational wave and over intervals of time much shorter than a gravitational wave period, these deflections cause a characteristic pattern of apparent proper motions.

Let T be the difference in the arrival times of radio sources at antennas in different geographic locations on earth. Then, Pyne et al. (1996) consider the variations produced by a gravitational wave in the delay time T, interpreted as variations in source position. They consider a gravitational wave traveling toward $+z$, with the '+' polarization, and the observed proper motion μ of a radio source at position $(\theta,\ \phi)$ will be (Fig. 2.4)

$$\mu = \frac{1}{2} ph \sin(p\eta) \sin(\theta)(\hat{\theta}\cos 2\phi - \hat{\phi}\sin 2\phi) \tag{2.4}$$

where (θ, ϕ) are the usual polar and azimuthal angle, p is the angular frequency, η is the proper time, h is a parameter in metric perturbation. This effect is expected to be very small and is very

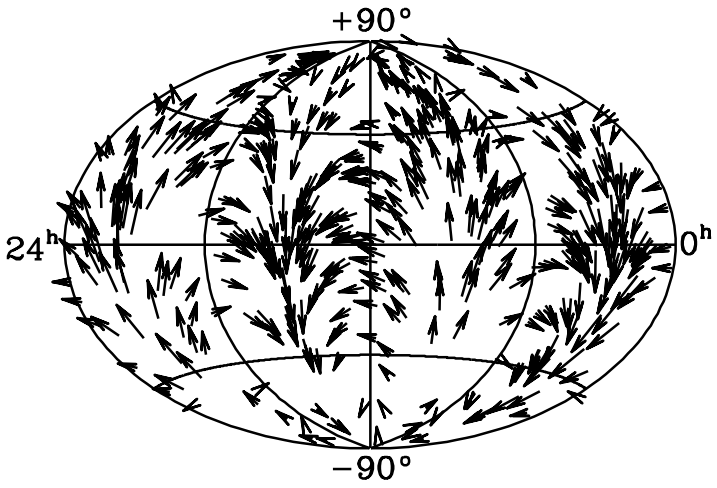

Figure 2.4: Proper motion due to a single gravitational wave (Gwinn et al. 1997).

unlikely to be measured by Gaia. However, Gaia may be able to place constraints on amplitude of such gravitational waves.

2.4 Anisotropic expansion of the universe

The standard model of cosmology rests on the assumption that the universe is homogeneous and isotropic, which is also known as Friedmann-Robertson-Walker (FRW) model. Here, we discuss the cases against the FRW model in two different scenarios: the Bianchi model and Lemaitre-Tolman-Bondi (LTB) void model. These universes are homogeneous but anisotropic.

By measuring the *cosmic parallax* in these two models, anisotropic expansion can be detected. Cosmic parallax is simply the temporal change of the angular separation between distant sources like quasars.

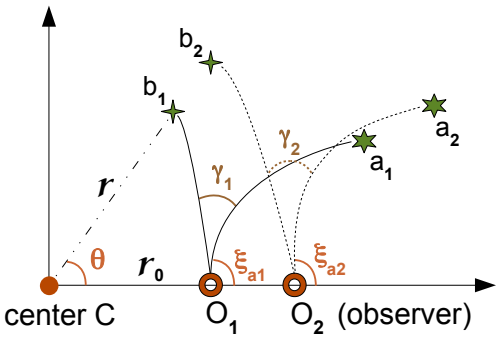

Figure 2.5: Cosmic parallax in LTB model (Quercellini et al. 2012).

1. **Cosmic parallax in LTB void model**: Referring to Fig. 2.5, consider two sources at location a_1, b_1 on the same plane with an angular separation γ_1 as seen from O (off-centre observer) both at distance X from C. After time Δt, the sources are at a_2, b_2 and the distances X, $X_{\rm obs}$ (corresponding to comoving coordinates r, r_0) will have increased by ΔX and $\Delta X_{\rm obs}$ respectively. Then the new angular separation will be γ_2. The variation

$$\Delta_t \gamma = \gamma_1 - \gamma_2 \tag{2.5}$$

is called the cosmic parallax. The numerical example by Quercellini et al. (2012) gives a value of the order of 10^{-2} μas yr^{-1}.

2. **Cosmic parallax in Bianchi model**: The metric of the Bianchi I model is given by

$$ds^2 = -dt^2 + a^2 dx^2 + b^2 dy^2 + c^2 dz^2 \tag{2.6}$$

where a, b and c are functions of time, t. Here, $H_X = \dot{a}/a$, $H_Y = \dot{b}/b$ and $H_Z = \dot{c}/c$ are the expansion rates along three spatial directions. Clearly, any measured deviation from isotropy results in different value of Hubble's constant. Let us consider two sources A and B in the sky located at some physical distance from observer O. Then if the expansion is homogeneous but anisotropic then the angular separation between two points changes with time as shown by Quercellini et al. (2012).

2.5 Peculiar proper motion

Galaxies in groups or clusters also have a motion towards the larger masses because of gravity. The peculiar motion of a galaxy is its velocity relative to the Hubble flow. The transverse component of this motion causes a proper motion of the galaxy which we call peculiar proper motion. In fact the recessional velocity of a galaxy is given by

$$v_r = H_0 d + v_{{\rm pec},r}$$

where $v_{{\rm pec},r}$ is the radial component of the peculiar velocity. The peculiar velocity of the Milky Way is ~600 km s^{-1}, but in rich galaxy clusters it may be as high as ~1500 km s^{-1} (Spark, 2000). The proper motion is then given by

$$\mu_{\rm pec} = \frac{v_{{\rm pec},t}}{d} \tag{2.7}$$

where $v_{{\rm pec},t}$ is the tangential component. However, this effect is random and will not give a systematic pattern of proper motion.

2.6 Quasar microlensing

For a quasar at $z = 3.0$ and for typical peculiar velocities of galaxies (v~600 km s^{-1}), its peculiar proper motion on the celestial sphere will be equivalent to

$$\mu = 0.02 \ \mu{\rm as/yr} \tag{2.8}$$

which is very small and hence the quasars can be assumed to be stationary.

However, recent observations (MacMillan, 2005) have shown that the proper motion values of some of these extragalactic objects seem to be far greater than Eq. (2.8).

It has been pointed out that the weak microlensing of these extragalactic objects by stars and dark bodies in our Galaxy can induce significant proper motions (Sazhin, 2011). In some cases the proper motions have been shown to be 10's of μas yr^{-1}. However the number of such events is estimated to be very low.

To better understand how the microlensing of quasars can occur, let us consider the figure below, where the symbols Q and L stand for quasar and lens respectively. D_Q and D_L are their respective distance in a flat FRW model.

If the quasar is at rest and the lens has a small motion v_L in the transverse direction then its proper motion is given by

$$\mu_L = \frac{v_L}{D_L} = -\frac{d\alpha}{dt}$$

The motion of the lens causes the image Q' of the source quasar to move resulting in a proper motion

$$\mu_{Q'} = \frac{d(\beta - \alpha)}{dt} = \frac{d\beta}{dt} + \mu_L$$

By considering a large number of lenses with the same Einstein radius θ_E, it can be shown that (Bachchan et al. 2015)

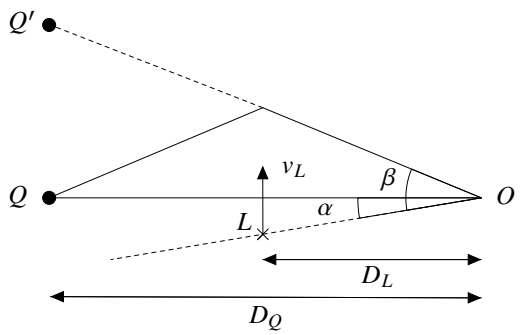

Figure 2.6: Lensing of quasar (Bachchan et al. 2015)

$$(\mu_{Q'})_{\text{RMS}} = (\mu_L)_{\text{RMS}} \times 2\sqrt{\tau} \tag{2.9}$$

where RMS stands for the root mean square value and $\tau = \pi\theta_E^2 N$ is the optical depth which gives the probability of the source Q being within the Einstein radius of some lens, where N is the surface density of lenses.

The value of τ for both the extragalactic case, where a galaxy acts as a lens, and the Galactic case, where stars and dark matter (such as planets or black holes) act as lenses, is much less than one (Belokurov & Evans, 2002). So, μ'_Q is also a very small number and cannot be measured by Gaia.

Chapter 3

Simulations

3.1 The Data

In the present work we used two different sets of quasars. The first set are the simulated quasars from the Gaia Universe Model Snapshot (GUMS) and the second set is the real quasars collected with certain constraints from different sources. The Gaia survey intends to reach a magnitude limit of $G_{\rm lim} = 20.7$ mag depending on the color of the object, with astrometric accuracies of about 25 μ as at $V = 15$ at the bright end only.

3.1.1 Gaia Universe Model Snapshot

The GUMS 'Gaia Universe Model Snapshot' is a model of the type of objects, their numbers, magnitudes and astrometric parameters that can be observed by Gaia (Robin et al. 2012). The simulated data are available at CDS (Centre de Données astronomiques de Strasbourg) via the link in the paper. The GUMS model generated $\sim 10^6$ quasars down to $G = 20$ and $\sim 3.7\times 10^7$ galaxies. In our work, we choose 5×10^5 quasars and 10^5 galaxies from this catalogue. When choosing galaxies, we restrict ourselves to more point-like galaxies in the redshift range $0.001 - 0.03$, selecting only Hubble type E2, E-S0, Sa and Sb.

3.1.2 Initial Gaia Quasar List

The second quasar catalogue that we used is the Initial Gaia Quasar List (IGQL) (Véron-Cetty & Véron 2010; Souchay et al. 2012; Andrei et al. 2009; Shen et al. 2011; Pâris et al. 2014; Andrei et al. 2012). It is a compilation of QSOs from the literature. The catalogue consists of $\sim 1.25\times 10^6$ objects of which $\sim 2\times 10^5$ are the defining sources. Objects brighter than magnitude 10 and astrometric accuracies less than one arcsecond were excluded from the catalogue. The all sky distribution of quasars is not homogeneous: it is densely populated in the northern hemisphere whereas the density is very thin in the southern hemisphere (Fig. 4 in Bachchan et al. 2015).

For both the GUMS and IGQL quasar sets, we assume that around 3300 of them have accurate VLBI positions. We assume this number as ICRF-2 currently has 3414 sources.

3.2 Simulation of quasars

Quasars (QSOs) are basically active galactic nuclei (AGNs) at the centres of which lie the supermassive black holes (SMBHs) surrounded by accretion disks and broad emission line regions. The central region may also be surrounded by dust arranged in a toroidal-like distribution. All these structures differ in energy. Popovic et al. (2012) have found that perturbations in the inner structure can cause a significant offset to the photocentre of the quasar which depends on the characteristics of perturbation and accretion disk as well as on the structure of the torus.

We assume the variability to be of the order of 100 μas. Since, the photocentric variation can be in any direction, we assume a Markov chain model to account for the variability on timescales of 2 and 10 years. We generated the photocentre positions based on the method given in Pasquato et al. (2011) which results in random variations in positions at time t_i can be generated by

$$\begin{bmatrix} \Delta\alpha_*(t_i) \\ \Delta\delta(t_i) \end{bmatrix} = e^{-\Delta t_i/\tau} \begin{bmatrix} \Delta\alpha_*(t_{i-1}) \\ \Delta\delta(t_{i-1}) \end{bmatrix} + \begin{bmatrix} g_i^{\alpha_*} \\ g_i^{\delta} \end{bmatrix}, \tag{3.1}$$

where

$$\Delta t_i = t_i - t_{i-1} \quad \text{and} \quad g_i^{\alpha_*},\ g_i^{\delta} \sim N(0, \sigma_i) \tag{3.2}$$

with

$$\sigma_i = \sigma_{\rm var}\sqrt{1 - \exp(-2\Delta t_i/\tau)}\,. \tag{3.3}$$

$\sigma_{\rm var}$ is the standard deviation of the random variations $\Delta\alpha_*(t)$ and $\Delta\delta(t)$. τ is the characteristic time, the time after which the correlation function decreases by the factor e. To account for the Solar System acceleration, we simulate a proper motion pattern of the form (Kopeikin & Makarov, 2006)

$$\begin{aligned} \mu_{\alpha^\star} &= -\tilde{a}_1 \sin\alpha + \tilde{a}_2 \cos\alpha \\ \mu_\delta &= -\tilde{a}_1 \cos\alpha \sin\delta - \tilde{a}_2 \sin\alpha \sin\delta + \tilde{a}_3 \cos\delta \end{aligned} \tag{3.4}$$

where $\tilde{\boldsymbol{a}} = \mathbf{a}/c$. We assumed $\tilde{\boldsymbol{a}} = (4.3, 0, 0)$ μas yr^{-1} in Galactic coordinates.

3.3 Simulation of galaxies

The galaxies are basically chosen to study any measurable effect of cosmological proper motion at low redshift where quasars are fewer in number. For this we calculated the shift in position using Eq. (2.2) and Eq. (2.3). We choose $v = 369$ km s^{-1}, $\Omega_m = 0.3$ and $\Omega_\Lambda = 0.7$. The proper motion components are then obtained by projecting this velocity on the tangent plane defined by the unit vector in the direction of the CMB antapex. We also added random peculiar proper motion component following Eq. (2.7) corresponding to a typical peculiar velocity of $v = 750$ km s^{-1} and again compute the proper motion components from the line-of-sight comoving distance.

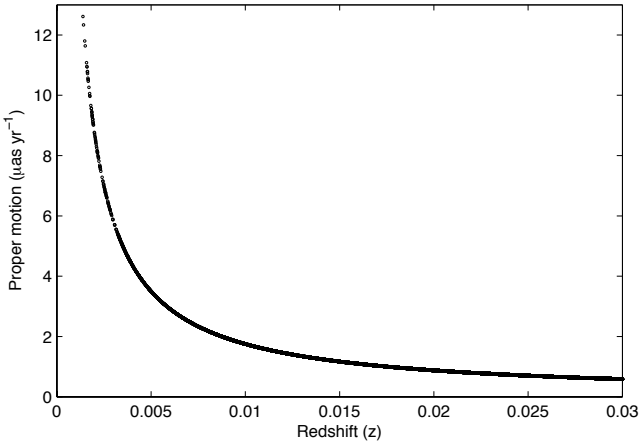

Figure 3.1: Variation of μ_0 with z

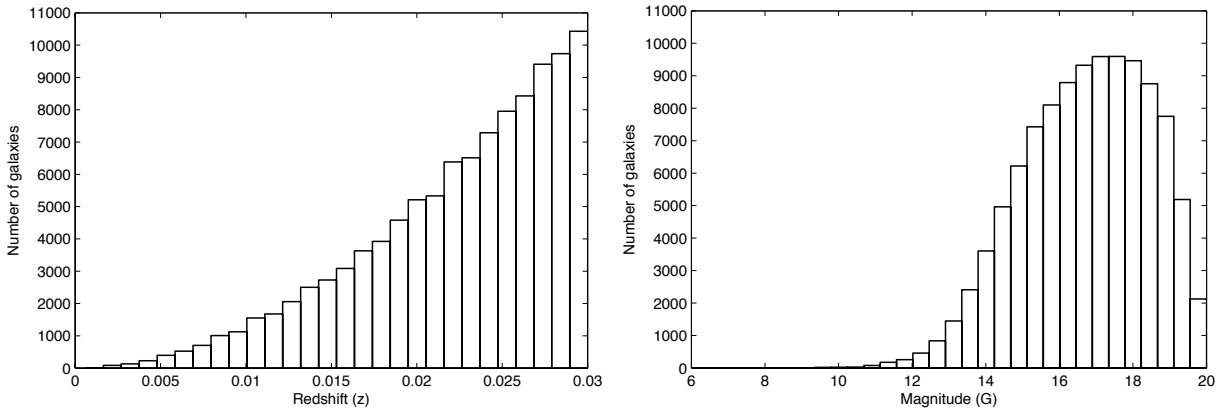

Figure 3.2: (a) Histogram of No. of galaxies vs z and (b) No. of galaxies vs magnitude

We selected galaxies in the range $0.001 \leq z \leq 0.03$ as μ_0 decreases with increase in z (Fig. 2.1). The histogram of z (Fig. 3.2a) shows that the number of galaxies increases with increase in z. At bright magnitudes there are very few galaxies, but the numbers increase rapidly for fainter magnitudes However, as the Gaia is a magnitude limited instrument, the number of galaxies detected gradually decreases as we can see beyond magnitude 17.5 in Fig. 3.2b.

3.4 Determining the reference frame and acceleration

In the Gaia astrometric model, the sources are constrained to move with uniform space velocity and when the angular measurements by Gaia are combined with such an astrometric model, the resulting reference frame has six degrees of freedom: three orientation parameters, $\boldsymbol{\varepsilon}$, because of the undefined origin of the reference frame and three spin parameters, $\boldsymbol{\omega}$, because of its rotation about an axis. When these corrections are applied to the AGIS frame, the resulting frame will be the optical realization of ICRF. For the calculation of $\boldsymbol{\varepsilon}$, $\boldsymbol{\omega}$ and acceleration, $\boldsymbol{a}$, we use the method as described in Lindegren (2007). Here, a quick receipe of the necessary relations involved are given.

Let,

$$\begin{aligned} t_0 &= \text{source reference epoch,} \\ t_1 &= \text{frame reference epoch} \\ (\alpha,\ \delta) &= \text{coordinate of a source in frame G at } t_0, \\ (\mu_{\alpha*},\ \mu_\delta) &= \text{proper motion of the source in frame G at } t_0, \\ (\omega_x,\ \omega_y,\ \omega_z) &= \text{x-, y-, z - component of spin and} \\ (\epsilon_x,\ \epsilon_y,\ \epsilon_z) &= \text{x-, y-, z - component of orientation,} \end{aligned}$$

Then, the total spin and the total orientation errors can be defined as

$$\omega = \left(\omega_x^2 + \omega_y^2 + \omega_z^2\right)^{1/2}, \quad \epsilon = \left(\epsilon_x^2 + \epsilon_y^2 + \epsilon_z^2\right)^{1/2}$$

The normal matrix at $(\alpha,\ \delta)$ is

$$[\boldsymbol{p} \quad \boldsymbol{q} \quad \boldsymbol{r}] = \begin{bmatrix} -\sin\alpha & -\sin\delta\cos\alpha & \cos\delta\cos\alpha \\ \cos\alpha & -\sin\delta\sin\alpha & \cos\delta\sin\alpha \\ 0 & \cos\delta & \sin\delta \end{bmatrix}$$

The first column of above matrix is $\boldsymbol{p}$, second column is $\boldsymbol{q}$ and the third column is $\boldsymbol{r}$, the position vector of the source in system G. The position vector of the source in system E at any arbitrary time t (which can also be t_0) is given by

$$\tilde{\boldsymbol{r}} = (\mathsf{E}'\mathsf{G})\boldsymbol{r} \tag{3.5}$$

where $(\mathsf{E}'\mathsf{G}) = f(\epsilon, \omega)$ is the rotation matrix from G to E frame. So, the key point here is to find $\boldsymbol{\epsilon}$ and $\boldsymbol{\omega}$ first which is described next.

The proper motion components in E is given by:

$$\tilde{\mu}_{\alpha*} = \tilde{\boldsymbol{p}}'(\mathsf{E}'\mathsf{G})(\boldsymbol{p}\mu_{\alpha*} + \boldsymbol{q}\mu_\delta - \mathsf{G}'\boldsymbol{\omega} \times \boldsymbol{r}) \tag{3.6}$$

$$\tilde{\mu}_\delta = \tilde{\boldsymbol{q}}'(\mathsf{E}'\mathsf{G})(\boldsymbol{p}\mu_{\alpha*} + \boldsymbol{q}\mu_\delta - \mathsf{G}'\boldsymbol{\omega} \times \boldsymbol{r}) \tag{3.7}$$

The spin parameter $\boldsymbol{\omega}$ is determined by the GAIA_QUASAR's which have well determined proper motion. Further, due to the acceleration of the Solar System barycentre towards the Galactic centre, these quasars contain a streaming like motion. If unit vector $\boldsymbol{r}$ is the position of a quasar on the sky then its apparent proper motion at $\boldsymbol{r}$ is given by

$$\boldsymbol{\mu} = (\boldsymbol{U} - \boldsymbol{r}\boldsymbol{r}')\boldsymbol{g}c^{-1} \tag{3.8}$$

where the acceleration is in units of proper motion $|\boldsymbol{a}| = |\boldsymbol{g}|c^{-1} = 4.3\ \mu as\ yr^{-1}$ and $\boldsymbol{U} - \boldsymbol{r}\boldsymbol{r}'$ is a tensor projection on the plane of the sky, normal to $\boldsymbol{r}$. If $\boldsymbol{r} = \boldsymbol{r}_0$, the barycentric coordinate direction at the source reference epoch, then the proper motion components of these quasars in the E frame can be directly found as

$$\tilde{\mu}_{\alpha*} = \tilde{\boldsymbol{p}}'(\mathsf{E}'\boldsymbol{a}) \tag{3.9}$$
$$\tilde{\mu}_{\delta} = \tilde{\boldsymbol{q}}'(\mathsf{E}'\boldsymbol{a}) \tag{3.10}$$

Comparing Eq. (3.6) with Eq. (3.9) and Eq. (3.7) with Eq. (3.10), we find that the residuals are

$$\begin{aligned} R_{\mu\alpha*} &= \tilde{\boldsymbol{p}}'(\mathsf{E}'\mathsf{G})(\boldsymbol{p}\mu_{\alpha*} + \boldsymbol{q}\mu_{\delta} - \mathsf{G}'\boldsymbol{\omega} \times \boldsymbol{r}) - \tilde{\boldsymbol{p}}'(\mathsf{E}'\boldsymbol{a}) \\ R_{\mu\delta} &= \tilde{\boldsymbol{q}}'(\mathsf{E}'\mathsf{G})(\boldsymbol{p}\mu_{\alpha*} + \boldsymbol{q}\mu_{\delta} - \mathsf{G}'\boldsymbol{\omega} \times \boldsymbol{r}) - \tilde{\boldsymbol{p}}'(\mathsf{E}'\boldsymbol{a}) \end{aligned} \tag{3.11}$$

Similarly, for VLBI_QUASAR's whose positions are known in E frame at the VLBI reference epoch t_2, the residuals are given by

$$\begin{aligned} R_{\alpha} &= \tilde{\boldsymbol{p}}' \left((\mathsf{E}'\mathsf{G})\boldsymbol{r} - \boldsymbol{r}_2^{(ICRS)} \right) - \tilde{\boldsymbol{p}}'(\mathsf{E}'\boldsymbol{a})(t_0 - t_2) \\ R_{\delta} &= \tilde{\boldsymbol{q}}' \left((\mathsf{E}'\mathsf{G})\boldsymbol{r} - \boldsymbol{r}_2^{(ICRS)} \right) - \tilde{\boldsymbol{q}}'(\mathsf{E}'\boldsymbol{a})(t_0 - t_2) \end{aligned} \tag{3.12}$$

where $\boldsymbol{r}_2^{(ICRS)}$ is the position calculated from ICRS data at t_2 in E frame. The partial derivatives of Eq. (3.11) and Eq. (3.12) with respect to $\mathsf{E}'\boldsymbol{\epsilon}$, $\mathsf{E}'\boldsymbol{\omega}$ and $\mathsf{E}'\boldsymbol{a}$ can be trivially obtained and used in a least squares solution to find the unknown frame rotation and acceleration parameters. The design equation is

$$\boldsymbol{A}\boldsymbol{x} = \boldsymbol{b} \tag{3.13}$$

which leads to the normal equations

$$\boldsymbol{A}^T\boldsymbol{A}\boldsymbol{x} = \boldsymbol{A}^T\boldsymbol{b} \tag{3.14}$$

The solution of which is given by (using standard factorization scheme e.g. SVD and Cholesky)

$$\boldsymbol{x} = [\boldsymbol{A}^T\boldsymbol{A}]^{-1}\boldsymbol{A}^T\boldsymbol{b} \tag{3.15}$$

where,

$$\boldsymbol{x} = \begin{pmatrix} \boldsymbol{\epsilon} \\ \boldsymbol{\omega} \\ \boldsymbol{a} \end{pmatrix}, \quad A = \begin{pmatrix} \frac{\partial R_\alpha}{\partial \mathsf{E}'\boldsymbol{\epsilon}} & \frac{\partial R_\alpha}{\partial \mathsf{E}'\boldsymbol{\omega}} & \frac{\partial R_\alpha}{\partial \mathsf{E}'\boldsymbol{a}} \\ \frac{\partial R_\delta}{\partial \mathsf{E}'\boldsymbol{\epsilon}} & \frac{\partial R_\delta}{\partial \mathsf{E}'\boldsymbol{\omega}} & \frac{\partial R_\delta}{\partial \mathsf{E}'\boldsymbol{a}} \\ \frac{\partial R_{\mu\alpha*}}{\partial \mathsf{E}'\boldsymbol{\epsilon}} & \frac{\partial R_{\mu\alpha*}}{\partial \mathsf{E}'\boldsymbol{\omega}} & \frac{\partial R_{\mu\alpha*}}{\partial \mathsf{E}'\boldsymbol{a}} \\ \frac{\partial R_{\mu\delta}}{\partial \mathsf{E}'\boldsymbol{\epsilon}} & \frac{\partial R_{\mu\delta}}{\partial \mathsf{E}'\boldsymbol{\omega}} & \frac{\partial R_{\mu\delta}}{\partial \mathsf{E}'\boldsymbol{a}} \end{pmatrix} \quad \text{and} \quad \boldsymbol{b} = \begin{pmatrix} R_\alpha \\ R_\delta \\ R_{\mu\alpha} \\ R_{\mu\delta} \end{pmatrix}$$

This implementation has been called 'FrameRotator' in the Gaia data processing.

There is another implementation called 'ExtendedFrameRotator' which estimates the cosmological proper motion using galaxies as mentioned in Sect. 2.2. In this model, we use the ϵ and ω based on 5×10^5 quasars from 'FrameRotator' as fixed input. The extragalactic galaxies also have a streaming like motion ($\mu = 4.3$ μas yr^{-1}) towards the Galactic centre like quasars. So, the net proper motion of these galaxies consist of the cosmological proper motion and Galactocentric acceleration, i.e.,

$$\mu = \mu_{\rm Gal} + \mu_{\rm cos} = \frac{a}{c} + \frac{v}{d} \sin\beta$$

where $\mu_{\rm Gal}$ is the Galactic proper motion given by Eq. (2.1) and $\mu_{\rm cos}$ is cosmological proper motion given by Eq. (2.2).

Chapter 4

Results and discussion

4.1 Galactocentric acceleration

We run 100 different realizations of the various simulation cases using the nominal Gaia observation noise and a nominal attitude noise of 10 μas. In each case, a first simulation is done using quasars

Table 4.1: Various cases considered in the simulation

Data Set	Case	Characteristic Time τ [yr]	VLBI_ QUASAR [μas]	GAIA_ QUASAR [μas]
Case A	GUMS	–	0	0
Case B	GUMS	2	100	100
Case C	GUMS	10	100	100
Case D	IGQL	–	0	0

to accurately determine the reference frame parameters, $\boldsymbol{\epsilon}$ and $\boldsymbol{\omega}$, and the acceleration of the Solar System, $\boldsymbol{a}$.

For Case A the mean value of Galactocentric acceleration is $|\boldsymbol{a}| = 4.304$ μas yr^{-1} with a standard deviation and mean formal error of $\sim$0.26 μas yr^{-1} compared to the input value of 4.3 μas yr^{-1}. This shows that a can be well determined to a few percent.

The addition of photocentric variability in Cases B and C do not alter the solution for a significantly and we get $|\boldsymbol{a}| = 4.308$ μas yr^{-1}. However, the standard deviation and the mean formal error increases slightly.

The use of IGQL dataset in Case D gives ($|\boldsymbol{a}| = 6.049$ μas yr^{-1}) however, the standard deviation and the formal errors do not change very much from Case A which is due to the non-uniform sky distribution of the IGQL data. The spin parameter ($\boldsymbol{\omega}$) is also poorly estimated. The IGQL data will be used in the early Gaia processing so the results should be interpreted carefully. Later, with the

detection of more quasars by Gaia, the IGQL catalogue will become homogeneous and the results will be more profound converging towards cases A, B and C.

4.2 Motion relative to Cosmic Microwave Background

First we determine $\boldsymbol{\epsilon}$ and $\boldsymbol{\omega}$ using the quasar simulations, which are then fixed input for these secondary simulations. We then perform two different simulations

- First, we determine the instantaneous velocity of the Solar System with respect to CMB ($v_{\rm CMB}$) together with the acceleration assuming the Hubble constant is known.
- Second, the Hubble constant is determined together with the acceleration term assuming the CMB velocity is known.

These two estimates of acceleration are done for a consistency check with the value determined from the quasar data. We found that the acceleration using galaxies do not change significantly when compared to that from quasars, but as fewer sources are used in this case the precision should decrease by $\sqrt{5}$.

However, the standard deviation and mean formal errors have increased by factors of ∼1.5 and ∼1.8 respectively, for Case A, which is due to the difference in the number of objects used. This discrepancy is probably due the lack of variability in the galaxy observations and that the galaxies are slightly brighter than the quasars (the number of galaxies peaks at ∼17 G magnitude). Also, the centroiding accuracy of galaxies is uncertain and requires further study.

We also give the recovered components of the $v_{\rm CMB}$, magnitude and direction. We started with $(l, b) = (263.99°, 48.26°)$ and $|\boldsymbol{v}| = 369$ km s^{-1} in the simulations. The recovered values are in good agreement in all the simulations. The magnitude of the standard deviation is ∼100 km s^{-1} while the magnitude of the mean formal error is ∼170 km s^{-1}. These errors are relatively large as we have used only 10^5 objects in the range $0.001 < z < 0.03$ while the largest contribution is from $z < 0.01$. The results for case D are less good because $\boldsymbol{\epsilon}$ and $\boldsymbol{\omega}$ are less accurate using the IGQL quasars.

Similarly, for the Hubble constant the recovered mean values are in good agreement in all simulations. Again the errors are relatively large, the standard deviation is about 11-12 km s^{-1} Mpc^{-1} while the mean formal error is of the order of 18 km s^{-1} Mpc^{-1}. Clearly, detecting more sources in the low redshift range $z < 0.01$ and with better centroiding accuracy would greatly improve these results.

The redshift dependent cosmological proper motion pattern due to $v_{\rm CMB}$ might be just about measurable. We alo reviewed other proper motion effects which are not strong enough to be detected by Gaia.

4.3 Conclusions and future work

The main conclusions of this work are:

1. Photocentric variability of quasars do not significantly degrade the quality of the reference frame.
2. The interpretation using IGQL data should be done carefully because of its inhomogeneous distribution at the moment.
3. Of the various proper motion patterns examined, only the Galactocentric acceleration definitely be measured by Gaia. In principle, the motion relative to the CMB is also within reach of Gaia, but only if accurate centroiding on galaxies is possible. For the future work we intend to develop a method to find the centroiding accuracy of extended objects, i.e., galaxies and component thereof.

References

[1] Aghanim N. et al, *Planck 2013 results. XXVII. Doppler boosting of the CMB: Eppur si muove*, A&A, **571**, A27 (2014)

[2] Andrei A. H. et al, *The large quasar reference frame (LQRF). An optical representation of the ICRS*, A&A, **505**, 385-404 (2009)

[3] Andrei A. H. et al, *Gaia initial QSO catalogue: The variability and compactness indexes*, Proceedings of the Annual meeting of the French Society of Astronomy and Astrophysics, 61-66 (2012)

[4] Bachchan R. K., Hobbs D., Lindegren L. *The Gaia reference frame amid quasar variability and proper motion patterns in the data*, A&A (2015) (to be submitted)

[5] Bastian U., *GAIA-CA-SP-ARI-BAS-003-06: Reference Systems, Conventions and Notations for Gaia* (2007)

[6] Bastian U., *Proceedings of the RGO-ESA Workshop Future Possibilities for Astrometry in Space* (ESA SP), **379**, 99 (1995)

[7] Belokurov V. A., Evans E. W., *Astrometric microlensing with the Gaia satellite*, MNRAS, **331**, 649-665 (2002)

[8] Capitaine A., *Weak Gravitational Lensing by Large Scale Structure*, ARA&A, **41**, 645 (2003)

[9] Capitaine A., *Micro-arcsecond Celestial Reference Frames: definition and realization - Impact of the recent IAU Resolutions*, RAA, **12**, **8**, 1162-1184 (2003)

[10] Fixsen D. J., *The Cosmic Microwave Background Spectrum From The Full COBE Firas Data Set*, AJ, **473**, 576-587 (1996)

[11] Green R. M., *Spherical Astronomy*, Cambridge University Press (1985)

[12] Gwinn C. R. et al., *Quasar proper motion and low-frequency gravitational wave*, ApJ, **485**, 87-91 (1997)

[13] Hu F. X. et al., *Orientation of Galaxies in the Local Supercluster: A Review*, Ap&SS, **302**, 43-59 (2006)

[14] Jacobs C. S., Arias, F., Boboltz, D., et al., *The ICRF3 Roadmap to the next generation International Celestial Reference Frame*, American Astronomical Society Meeting (2014)

[15] Klioner S., *A Practical Relativistic Model for Microarcsecond Astrometry in Space*, AJ, **125**, 1580 (2003)

[16] Kopeikin, S. M. and Makarov, V. V., *Astrometric Effects of Secular Aberration*, AJ, **131**, 1471 (2006)

[17] Kovalevsky J., *Fundamentals of Astrometry*, Cambridge University Press (2004)

[18] Lindegren L., *Mathematical framework for the AGIS System Orientation* (2007)

[19] Lindegren, L., Lammers, U., Hobbs, D., et al., *The astrometric core solution for the Gaia mission. Overview of models, algorithms, and software implementation*, A&A, **538**, A78 (2012)

[20] Loeb A., *Direct measurement of cosmological parameters from the cosmic deceleration of extragalactic objects*, AJ, **499**, 111-114 (1998)

[21] MacMillan D. C., *Future Directions in High Res- olution Astronomy: The 10th Anniversary of the VLBI*, ASP Conf. Ser. **340**, 477 (2005)

[22] Pâris, I., *The Sloan Digital Sky Survey quasar catalog: tenth data release*, A&A, **563**, A54 (2014)

[23] Pasquato E. et al., *Limits in astrometric accuracy induced by surface brightness asymmetries in red supergiant stars*, A&A, **532**, A13 (2011)

[24] Perryman M. et al., *The Gaia Inertial Reference Frame And The Tilting Of The Milky Way Disk*, ApJ, **789**, 166 (2014)

[25] Popovic L. C. et al., *Photocentric variability of quasars caused by variations in their inner structure: consequences for Gaia measurements*, A&A, **538**, A107 (2012)

[26] Pyne T. et al., *Gravitational radiation and very long baseline interferometry*, ApJ, **465**, 566-577 (1996)

[27] Quercellini C. et al., *Real Time Cosmology*, Physics Reports, **521**, 95-134 (2012)

[28] Robin A. C. et al., *Gaia Universe model snapshot, A statistical analysis of the expected contents of the Gaia catalogue*, A&A, **543**, A100 (2012)

[29] Sazhin M. V. et al., *Apparent motions of quasars due to microlensing*, Astronomy Reports, **55**, 954 (2011)

[30] Shen, Y. et al., *A Catalog of Quasar Properties from Sloan Digital Sky Survey Data Release 7*, ApJS, **194**, 45 (2011)

[31] Souchay, J. et al, *The second release of the Large Quasar Astrometric Catalog (LQAC-2)*, A&A, **537**, A99 (2012)

[32] Sparke L. S. and Gallagher, J. S., *Galaxies in the universe : an introduction*, Cambridge University Press, UK (2000)

[33] van Altena W. F., *Astrometry for Astrophysics*, Cambridge University Press (2012)

[34] Véron-Cetty, M.-P. and Véron, P., *A catalogue of quasars and active nuclei: 13th edition*, A&A, **518**, A10 (2010)

[35] Weinberg S., *Gravitation and Cosmology, Principles and Applications of the General Theory of Relativity*, John Wiley and Sons, New York (1972)

[36] web[1]: http://aa.usno.navy.mil/faq/docs/ICRS_doc.php

[37] web[2]: http://aa.usno.navy.mil/faq/docs/ICRS_doc.php

[38] web[3]: http://www.rssd.esa.int/SA/GAIA/docs/info_sheets/IN_astrometric_instrument.pdf

[39] web[4]: http://www.rssd.esa.int/SA/GAIA/docs/info_sheets/IN_gaia_telescope.pdf

Astronomy & Astrophysics manuscript no. quasarVariability
November 12, 2015

The Gaia reference frame amid quasar variability and proper motion patterns in the data

R. K. Bachchan[1], D. Hobbs[1] and L. Lindegren[1]

Lund Observatory, Lund University, Box 43, SE-22100 Lund
e-mail: rajesh, david, lennart@astro.lu.se

Received ..... / Accepted .....

ABSTRACT

Context. Gaia's very accurate astrometric measurements will allow the International Celestial Reference Frame (ICRF) to be improved by a few orders of magnitude in the optical. Several sets of quasars are used to define a kinematically stable non-rotating reference frame with the barycentre of the Solar System as its origin. Gaia will also observe a large number of galaxies which could obtain accurate positions and proper motions although they are not point-like.
Aims. The optical stability of the quasars is critical and we investigate how accurately the reference frame can be recovered. Various proper motion patterns are also present in the data, the best known is the acceleration of the Solar System, presumably, towards the Galactic centre. We review some other less-well-known effects that are not part of standard astrometric models.
Methods. We model quasars and galaxies using realistic sky distributions, magnitudes and redshifts. Position variability is introduced using a Markov chain model. The reference frame is determined using the algorithm developed for the Gaia mission which also determines the acceleration of the Solar System. We also test a method to measure the velocity of the Solar System barycentre in a cosmological frame.
Results. We simulate the recovery of the reference frame and the acceleration of the Solar System and conclude that they are not significantly disturbed in the presence of quasar variability which is statistically averaged. However, the effect of a non-uniform sky distribution of the quasars can result in a correlation between the reference frame and acceleration which degrades the solution. Our results suggest that an attempt should be made to astrometrically determine our velocity relative to the CMB, which in principle could allow the determination of the Hubble parameter.

Key words. Astrometry – reference frames – cosmology: observations – galaxies: general – quasars: general – Methods: data analysis – Space vehicles: instruments

1. Introduction

Gaia is an astrometric satellite launched in late 2013 and designed to produce a three-dimensional map of our Galaxy from which its composition, formation and evolution can be reconstructed. It will measure the positions, proper motions and parallaxes of at least one billion stars in the Milky Way. In addition, Gaia will detect thousands of exoplanets, asteroids and around half a million distant quasars in the optical spectrum. Since the accuracy is at the micro-arcsecond level, these precise measurements help to improve the International Celestial Reference Frame (ICRF) in the optical by a few orders of magnitude. It will also provide a number of new tests of the general theory of relativity.

The ICRF (Ma et al. 1998) is a quasi-inertial reference frame which was originally defined by the measured positions of 212 extragalactic radio sources derived from ground based Very Long Baseline Interferometry (VLBI), and has its reference point at the barycentre of the Solar System. In general relativity there is no true inertial reference frame, however, the extragalactic sources (quasars) used to define the ICRF are so far away that any net angular motion is almost zero. The ICRF is now the standard reference frame used to define the positions of astronomical objects. It has been adopted by International Astronomical Union since 1998 (Ma et al. 1998). In 2009, the second realization, ICRF2 (Ma et al. 2009), was adopted including improved models and concepts and was based on 3414 compact astronomical sources. ICRF2 defines the reference frame to an accuracy of 40 μas and includes 295 defining sources uniformly distributed on the sky and selected on the basis of positional stability and the lack of extensive intrinsic source structure.

The Hipparcos and Tycho catalogues (ESA 1997) currently serve as the corresponding optical realization of the International Reference System (ICRS) but will be superseded by the Gaia mission in the coming years (Mignard 2011). This frame must be constructed with the same principles as the ICRS, i.e. overall a kinematically non-rotating system with the same orientation as the ICRF. It is estimated that Gaia will astrometrically measure some 500 000 quasars and their repeated measurement over the estimated five year mission will lead to a new kinematically defined inertial reference frame in the optical.

Quasars located at the centre of distant active galaxies are characterized by extremely compact and bright emission. They are at cosmological distances and therefore show negligible transverse motion. However, recent observations (Taris et al. 2011; Porcas 2009; Kovalev et al. 2008) of Active Galactic Nuclei (AGNs) and theoretical studies (Popović et al. 2012) indicate that variability in the accretion disk and dusty torus surrounding the central black hole can cause photocentre shifts of up to the milliarcsec level, so it is probable that quasar variability will affect the reference frame as well. This paper investigates the sta-

tistical impact of variability on the Gaia reference frame based on simulated astrometric observations.

Another interesting aspect is the acceleration of the Solar System first pointed out by Bastian (1995) which causes a pattern of proper motions that can be solved for while determining the reference frame orientation and spin parameters. We present an estimate of how well the acceleration vector can be determined based on realistic Gaia simulations which also assess the impact of quasar variability. In addition to this effect there may be several more subtle effects present in the real data. Many of these will be small, nevertheless, it is interesting to review and compare them and if deemed large enough we can simulate them together with the acceleration of the Solar System to assess their impact on the solution and the potential to disentangle the different effects.

The organization of the paper is as follows: Section 2 presents various proper motion effects that could have an impact on the Gaia measurements and we quantify their respective magnitudes. In Sect. 3 we present the numerical simulations. In Sect. 4 we explain how the Gaia reference frame is determined together with the patterns of proper motion discussed in Sect. 2. In Sect. 5 the simulation results are presented and discussed and finally in Sect. 6 conclusions are given.

2. Proper motion effects in the Gaia data

Titov (2010) has noted that individual apparent proper motions of distant radio sources are generally attributed to the internal structure of AGNs. However, he points out that there are a number of other effects that could give rise to systematic apparent motions of quasars and we will briefly consider them here. The various sources of proper motion are summarized in Table 1. Note that the terminology used in the literature describing the different effects varies and can be inconsistent mainly due to the historical progression of the topics.

2.1. Photocentre variability

Perryman et al. (2014) considered the various sources of quasar instability. They concluded that the most important effect is optical photo-centric motion, where the internal structure of the AGN could result in variability typically less that 60 μas but up to 100 μas in extreme cases (Taris et al. 2011). In these simulations we consider the extreme case where these effects combine to produce maximum variability distortions of 100 μas. The time scales of quasar variability have been studied by Smith et al. (1993) and Taris et al. (2011) and found to range from 3–15 years, peaking between 6–9 years. We have chosen to use 2 and 10 years which represents roughly the range of time scales to which Gaia is sensitive, assuming a mission duration of 5 years.

Table 1. Table of various perspective effects. "o" refers to the effect being due to the observer's motion. "s" refers to the effect being due to the source's motion while "c" refers to the effect being of cosmological origin. We arbitrarily define the boundary between low and high z as a redshift of 1.0.

Effect	Origin	Description	Measurement method	Expected magnitude	Redshift dependence
Acceleration of the Solar System	o	Acceleration of the Solar System assumed to be towards the Galactic centre resulting in patterns of proper motion. However, the local group of galaxies and clusters of local supercluster will also contribute to the effect.	Astrometric	$\sim 4.3\ \mu$as yr^{-1}	None
Cosmological proper motion	o	Instantaneous velocity of the Solar System with respect to the CMB can cause distant extragalactic sources to undergo an apparent systematic proper motion.	CMB and astrometric	1–2 μas yr^{-1}	Increases at low z
Gravitational waves	o	Primordial gravitational waves produce systematic proper motions over the sky.	Dedicated detectors/ possibly astrometric	Unknown but probably $< 1\ \mu$as yr^{-1}	None
Transverse redshift drift/ Cosmic parallax	c	A temporal shift of the angular separation of distant sources can be used to detect an anisotropic expansion of the universe and results in a pattern of proper motions.	Astrometric	0.2 μas yr^{-1} (Bianchi) 0.02 μas yr^{-1} (LTB)	Increases at high z, decreases at very high z
Peculiar proper motion	s	Proper acceleration is the observed transverse acceleration of an object due to the local gravitational field.	Astrometric	Can be 10 μas yr^{-1} for Galactic clusters	None
Quasar microlensing	s	Weak microlensing can induce apparent motions of quasars.	Astrometry photometry	10's of μas yr^{-1} but is extremely rare	None

2.2. Acceleration of the Solar System

The Solar System's orbital velocity around the Galactic centre results in an aberration effect of about 2.5 arc-minutes (Perryman et al. 2014) in the direction of motion. The acceleration of the Solar System in its Galactic orbit causes this effect to change slowly, which results in a proper motion pattern for all objects on the sky (Bastian 1995; Kovalevsky 2003; Gwinn et al. 1997; Sovers et al. 1998; Klioner 2003; Kopeikin & Makarov 2006). This effect has also been referred to as secular aberration drift (Titov 2010). The effect is generally assumed to be towards the Galactic centre where most of the mass is concentrated but of course the unknown distribution of dark matter may affect the direction. The Galactocentric acceleration can be calculated as $a = v^2/r$, assuming a circular velocity $v = 223$ km s^{-1} and radius $r = 8.2$ kpc (Ghez et al. 2008). The resulting proper motion pattern is

$$\mu = \tilde{a} \sin\theta \,, \quad \tilde{a} = \frac{a}{c} = 4.3\ \mu\text{as yr}^{-1} \,, \tag{1}$$

where c is the speed of light and θ is the angular distance between the object and the Galactic centre (Bastian 1995). For objects within our Galaxy, the effect could be considerably smaller because only the relative acceleration matters. Kovalevsky (2003) argued that the time dependent aberration of stars in the Galaxy due to their own motion should also be included as a correction. This correction depends on the star's distance and location on the sky and can amount to hundreds of μas yr^{-1} close to the Galactic centre. However, this correction basically takes into account the nonlinear motion of the stars between the emission and the observation epochs and while the effect is valid it is not what Gaia is trying to measure. The Gaia measurements are for the position of the stars as seen by Gaia at the current epoch and not where they are, in this example, some 27 000 years later.

The local group and local supercluster also accelerate the barycentre of the Solar System similar to the Galactocentric acceleration. We have estimated $\tilde{a}$ for some 33 galaxies of the local group, using $a = Gm/r^2$ and the seven largest examples are listed in Table A. We see that the values of $\tilde{a}$ are very small (< 0.1 μas yr^{-1}) and will not be possible to measure with Gaia. We similarly calculate the value of $\tilde{a}$ for some clusters of the local supercluster and in this case too the values are found to be very small and not measurable by Gaia.

If we consider some non-axisymmetric potential for the Milky Way consisting of bulge, disk and halo along with spiral arms similar to the one used by Feng & Bailer-Jones (2013) then the acceleration vector will not exactly point towards the Galactic centre Instead, the acceleration vector was found, in the presence of spiral arms, to make an angle of 2.24° compared to the case with no spiral arms.

2.3. Cosmological proper motion

The instantaneous velocity of the Solar System with respect to the CMB will cause distant extragalactic sources to undergo an apparent systematic proper motion. The effect is referred to as cosmological or parallactic proper motion (Kardashev 1986). This effect will depend on the redshift z and fundamental cosmological parameters can in principle be determined from the motion. The velocity (v) of the Solar System with respect to the observable Universe produces a dipole pattern in the CMB temperature with $\Delta T/T = v/c$. Observations of CMB indicates that $v = 369 \pm 0.9$ km s^{-1} in the apex direction with Galactic longitude $l = 263.99°$ and latitude $b = 48.26°$ (Hinshaw et al. 2009; Planck Collaboration et al. 2014). This motion should produce a parallactic shift of all extragalactic objects towards the antapex at the angular rate

$$\mu = \frac{v}{d} \sin\beta \,, \tag{2}$$

where β is the angle between the source and apex directions and

$$d(z) = \frac{c}{H_0} \int_0^z \frac{dz'}{\sqrt{\Omega_m(1+z)^3 + \Omega_r(1+z)^4 + \Omega_k(1+z)^2 + \Omega_\Lambda}} \,, \tag{3}$$

is the transverse comoving distance, which for a flat universe

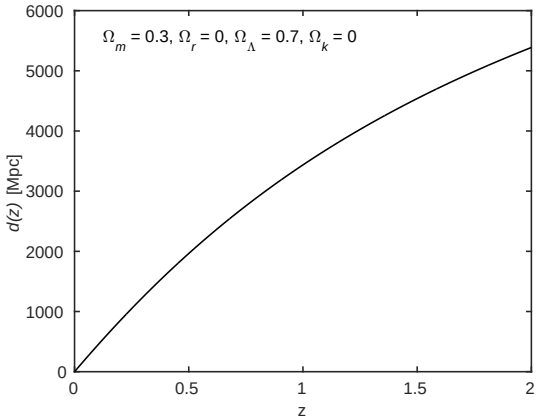

Fig. 1. Variation of comoving distance with redshift.

equals the line-of-sight comoving distance (Hogg 1999; Hobson et al. 2006; Weinberg 2008). The quantities Ω_m, Ω_r, Ω_k and Ω_Λ are the dimensionless energy densities of matter, radiation, curvature and cosmological constant respectively. For very low redshift ($z \ll 1$), $\mu \simeq (vH_0/cz)\sin\beta$, or 1–2 μas yr^{-1} for $z = 0.01$ (Kardashev 1986). In principle, this could be within the reach of Gaia, depending on the number of available objects and the precision of the observations.

Both the acceleration of the Solar System and the cosmological proper motion give rise to dipole patterns in the proper motions of distant objects. However, the former does not depend on the redshift, while the latter does, which makes it possible to separate the effects.

2.4. Primordial gravitational waves

Primordial gravitational waves could give rise to systematic proper motions over the sky, composed of second order transverse vector spherical harmonics (Gwinn et al. 1997). Changes in the space time metric due to gravitational waves alter the optical path length, preserves the sources brightness and intensity but produces oscillations in the apparent position of the source. If the interval of observation is shorter than the period of the gravitational wave then this will be seen as a systematic proper motion on the sky. Pyne et al. (1996) and Gwinn et al. (1997) have investigated in detail the low frequency observational constraints on gravitational waves, which could arise naturally in inflationary theories of cosmology. It is anticipated that Gaia is not sufficiently sensitive to detect gravitational waves directly but should be able to place upper limits on their energy density which is comparable to that of pulsar timing measurements (Book & Flanagan 2011).

2.5. Transverse redshift drift / Cosmic parallax

Kristian & Sachs (1966) and Titov (2009) have pointed out that an anisotropic expansion of the Universe would result in a distortion, as a function of redshift, of all distant objects on the celestial sphere in a particular direction. The effect gives a direct measurement of space time curvature, which is similar to a gravitational lens but in this case it is due to the cosmological curvature rather than a single body. The time dependent components of the distortion would result in patterns of proper motion which could be a function of the redshifts and can be measured in principle. Titov (2009) has shown that the dipole term does not vary significantly but the quadrupole term gradually increases with redshift and could be interpreted as an anisotropic Hubble expansion or as possible indicators of primordial gravitational waves in the early Universe.

Quercellini et al. (2009, 2012) use the term 'cosmic parallax' for the varying angular separation between any two distant sources, caused by the anisotropic expansion of the universe. They considered two different scenarios:

- Bianchi 1 models in which the observer is centrally embedded in an intrinsically anisotropic expansion of the early universe. In this case, the anisotropic stress of dark energy can induce an anisotropic expansion of the universe at late times which cannot be constrained by the CMB background measurements. Their simplified model, assuming an anisotropy of the order of 1%, give a proper motion pattern of about 0.2 μas yr^{-1}.
- LTB (Lemaitre-Tolman-Bondi) void models in which the observer is off-centre and the universe is inhomogeneous and isotropic. For the models considered by Quercellini et al. (2012), they derived effects of the order of 0.02 μas yr^{-1}.

2.6. Peculiar proper motion

In analogy to the peculiar motion of stars, which is defined as the star's velocity relative to the local standard of rest, the peculiar motion of a galaxy is its velocity relative to the Hubble flow. The transverse component of this motion causes a proper motion of the galaxy which we call peculiar proper motion. The typical velocities ($v_{\rm pec}$) are of the order of $\sim$ 600 km s^{-1}, but in rich galaxy clusters it may be as high as $\sim$ 1500 km s^{-1} (Sparke & Gallagher 2000). The proper motion is then given by

$$\mu_{\rm pec} = \frac{v_{\rm pec}}{d} \,, \tag{4}$$

or $\mu_{\rm pec} \simeq v_{\rm pec} H_0/cz$ for small redshifts. This gives a peculiar proper motion in the range 3–7 μas yr^{-1} at $z = 0.01$. The effect is random and is not expected to give a systematic pattern of proper motion.

2.7. Quasar microlensing

Belokurov & Evans (2002) have pointed that microlensing events can be detected by Gaia due to the brightening of the source stars. The optical depth is given by them as 10^{-7} and 2.5×10^{-5} for photometric and astrometric microlensing respectively and corresponds to about 1300 photometric and 25000 astrometric microlensing events respectively during the course of the nominal 5 year Gaia mission. The individual images of microlensed sources cannot be resolved by Gaia but the centroid shift along the trajectory of a source can be measured. In the case of stellar microlensing of quasars, the centroid shift can be tens of μas (Lewis & Ibata 1998).

If we consider that a source is a Quasar with zero proper motion ($\mu_Q = 0$), then by considering a large number of lensing objects with random proper motions it can be shown (see Appendix B) that

$$(\mu_{Q'})_{\rm RMS} = (\mu_L)_{\rm RMS} \times 2\sqrt{\tau} \tag{5}$$

where $(\mu_{Q'})_{\rm RMS}$ is the RMS value of the quasar proper motion, $(\mu_L)_{\rm RMS}$ is the RMS value of the lens proper motion and $\tau = \pi\theta_E^2 N$ is the probability that the source Q will be within the Einstein radius of some lens, which is also referred to as 'optical depth'. N is the number of lens and θ_E is the Einstein angle which we assumed to be same for all the lenses.

If we assume the number of galaxies is 0.05 Mpc^{-3}, a lens mass of 10^{11} M$_\odot$, a lens distance of 5 Gpc and source distance of 10 Gpc then the value of $\tau \sim 0.08$ in the extragalactic case. Similarly, in case of Galactic microlensing, if we take the number of sources as 0.1 pc^{-3}, a mass of 1 M$_\odot$, a lens distance of 5 kpc and a source distance of 10 kpc then $\tau \sim 10^{-6}$. Clearly, $(\mu_{Q'})_{\rm RMS} \ll 1$ in both cases. So even though a distant galaxy acting as a lens has a tiny motion in the transverse direction with respect to the observer, the source quasar being at rest, the apparent proper motion of the quasar is too small to be measured by Gaia and the same applies to the case of Galactic microlensing.

2.8. Other apparent motions of quasars

The peculiar proper motion of quasars is expected to be very small due to their large distances. For example, for a quasar at $z = 3$, $\mu_{\rm pec} = 0.02$ μas yr^{-1} according to Eqs. (3) and (4). This proper motion is very small and hence the quasars can in this respect be assumed to be stationary. However, radio observations of quasars have shown that a significant number of them have apparent proper motions exceeding 50 μas yr^{-1} (MacMillan 2005), Titov et al. (2011). Sazhin et al. (2011) have pointed out several possible causes, including apparent superluminal motions in radio jets, gravitational waves and weak microlensing by stars and dark bodies in our Galaxy. Sazhin et al. (2011) has given a number of examples of apparent motions due to microlensing and the order of proper motions in some cases has been shown to be several tens of μas yr^{-1}. However the number of such events is estimated to be very small.

3. Simulations

3.1. The data sets

In order to simulate the quasars and galaxies we take the positions, magnitudes and redshifts of the objects from the GUMS (Robin et al. 2012) simulated data set. This data set includes a realistic sky, magnitude and redshift distribution of around 1 million quasars and 38 million unresolved galaxies [1] expected to be seen by Gaia. As a significant fraction of the galaxies will not be observed by Gaia due to their extended structure, we focus on the simpler and most point like objects down to $G = 20$ magnitude by selecting only ellipticals and spirals (Hubble types E2, E-S0, Sa and Sb with bulge to total flux ratio of 1.0, 0.9, 0.56–0.57 and 0.31–0.32 respectively) in the redshift range 0.001 to

[1] 'Unresolved' here means that individual stars in a galaxy cannot be seen by Gaia. The galaxy as a whole is however often an extended object at the resolution of Gaia.

0.03. This results in just over 100 000 objects, which is sufficient for our simulations.

The GUMS data set of nearly 1 million quasars represent an idealized case i.e, those objects which in principle could be used for the frame determination assuming that they can be correctly classified by means of the Gaia observations (Bailer-Jones et al. 2008). We randomly selected half a million of quasars from the full dataset for our simulations.

As a very conservative alternative we also consider using the Initial Gaia Quasar List (IGQL; Andrei et al. 2009, 2012) which currently consists of around 1.2 million quasars compiled from various catalogues. It will be used in the early Gaia data processing to simplify the identification of quasars. IGQL contains a snapshot of the best information of optical quasars available just before the launch of the Gaia. The quasars in the IGQL are not uniformly distributed on the sky but there are a number of bands and high density regions corresponding to the various surveys used to compile it (Véron-Cetty & Véron 2010; Souchay et al. 2012; Andrei et al. 2009, 2012; Shen et al. 2011; Pâris et al. 2014). Notably, the IGQL is significantly lacking sky coverage in the southern hemisphere and the impact of this non-uniform distribution will be discussed in Sect. 5.

For both quasar data sets, a random subset of about 3300 objects are assumed to have accurate VLBI positions, simulating the ICRF2 catalogue.

3.2. Simulating quasar observations

To include the Galactocentric acceleration in these data sets we simulate a pattern of proper motions of the form (Kopeikin & Makarov 2006):

$$\begin{aligned} \mu_{\alpha^\star} &= -\tilde{a}_1 \sin\alpha + \tilde{a}_2 \cos\alpha \\ \mu_\delta &= -\tilde{a}_1 \cos\alpha \sin\delta - \tilde{a}_2 \sin\alpha \sin\delta + \tilde{a}_3 \cos\delta \end{aligned} \tag{6}$$

where $\mu_{\alpha^\star} = \mu_\alpha \cos\delta$ and $\tilde{\boldsymbol{a}} = (\tilde{a}_1, \tilde{a}_2, \tilde{a}_3)$ is the acceleration divide by speed of light, Eq. (1), in ICRS. We assumed acceleration components as $\tilde{\boldsymbol{a}} = (-0.236, -3.756, -2.080)$ μas yr^{-1} in ICRS which corresponds to $(4.3, 0, 0)$ μas yr^{-1} in Galactic coordinates, i.e. directed towards the Galactic centre.

To simulate quasar photocentric variability, we use a Markov chain with an exponentially decaying correlation (Pasquato et al. 2011; Chatfield 2013; Doob 1942) with a characteristic correlation time scale τ. This results in random variations in positions at time t_i that are both Gaussian and Markovian and generated by

$$\begin{bmatrix} \Delta\alpha_*(t_i) \\ \Delta\delta(t_i) \end{bmatrix} = e^{-\Delta t_i/\tau} \begin{bmatrix} \Delta\alpha_*(t_{i-1}) \\ \Delta\delta(t_{i-1}) \end{bmatrix} + \begin{bmatrix} g_i^{\alpha_*} \\ g_i^{\delta} \end{bmatrix}, \tag{7}$$

where $\Delta t_i = t_i - t_{i-1}$ and the $g_i^{\alpha_*}$ and g_i^{δ} are sampled from a Gaussian distribution with zero mean and standard deviation

$$\sigma_i = \sigma_{\rm var} \sqrt{1 - \exp(-2\Delta t_i/\tau)}\,. \tag{8}$$

$\sigma_{\rm var}$ is the standard deviation of the random variations $\Delta\alpha_*(t)$ and $\Delta\delta(t)$, which are used to perturb the source positions for each quasar independently. We assume photocentre variations of $\sigma_{\rm var} = 100\,\mu$as and $\tau = 2$ and 10 years (Sect. 2.1). Two examples of Markov chain photocentre variability are shown in Fig. 2.

3.3. Simulating galaxy observations

As explained in Sect. 3.1, we simulate only 100 000 galaxies (GAIA_GALAXY) from GUMS which are used for simulations involving redshift dependent proper motion patterns. This number is very conservative considering there are 38 million galaxies in the GUMS catalogue but we also restrict ourselves to a narrow redshift range (0.001 – 0.03) where the effect is strongest (see Figure 3). In this redshift range the angular diameter of a typical galaxy core (assuming a core diameter of 1 kpc) is between 46″ and 1.5″ respectively. In the simulation we assume that these galaxies can be observed with the same accuracies as the point-like sources. This assumption is certainly unrealistic, given their extended structures, but is adopted here pending a more detailed study of the centroiding accuracies for such objects. The purpose here is to investigate whether these patterns are potentially detectable by Gaia. Clearly increasing the redshift range will increase the number of objects with small angular diameter but the amplitude of the proper motion patterns also decreases at higher redshift.

To include the cosmological proper motion we calculate the shift in position based on the line-of-sight comoving distance using Eqs. (2) and (3) assuming a velocity of 369.0 km s^{-1} and a Hubble constant of 67.3 km s^{-1} Mpc^{-1}. The proper motion components are then obtained by projecting this velocity on the tangent plane defined by the unit vector in the direction of the CMB antapex. In addition, we calculate random proper motion components of the galaxies by assuming a velocity dispersion of $v = 750$km s^{-1} and again compute the proper motion components from the line-of-sight comoving distance. These different effects are simulated together with the Galactocentric acceleration using Eq. (6) but with the modified values for the coefficients.

3.4. Tools and other simulation parameters

For our simulations we have used AGISLab (Holl et al. 2012) which is a lightweight simulation tool used to help develop and test concepts and the corresponding algorithms for the Gaia data processing. AGISLab implements much of the functionality of the real Gaia data reduction software but, in addition, is able to generate simulated observations using realistic estimates of the observation noise as a function of magnitude. Using this tool, sets of true and noisy astrometric parameters can be generated for a range of different types of sources distributed on the celestial sphere. In addition, attitude parameters for Gaia can be modelled by fitting splines to the nominal scanning law of the mission. For both the source and attitude parameters, different initial systematic and random noise values can be added and are then compared to the true values as an iterative solution proceeds until an acceptable level of convergence is achieved. AGISLab generates the observations based on, for example, the satellite's CCD geometry and its orbit. Additionally, the direction to a source is computed using the full Gaia relativity model (Klioner 2003, 2004). A set of observation equations are used to construct the least-squares problem for the astrometric parameters using normal equations (Lindegren et al. 2012) which are then solved using a conjugate gradient algorithm described in Bombrun et al. (2012). In addition, to the conventional features of AGISLab we have also added the option to include Markov chain photocentre variability as a perturbation to the transit times on the Gaia CCD's. Finally, AGISLab contains a number of utilities to generate statistics and graphical output.

In the simulations presented here we use AGISLab without scaling down (see Holl et al. (2012)) the mission and assume an attitude modelling knot interval of 30 seconds. For the starting noisy astrometric parameters we use 100 mas random errors and 10 mas systematic errors while for the attitude parameters we assume a nominal attitude error of 10 μas. For the accuracy of

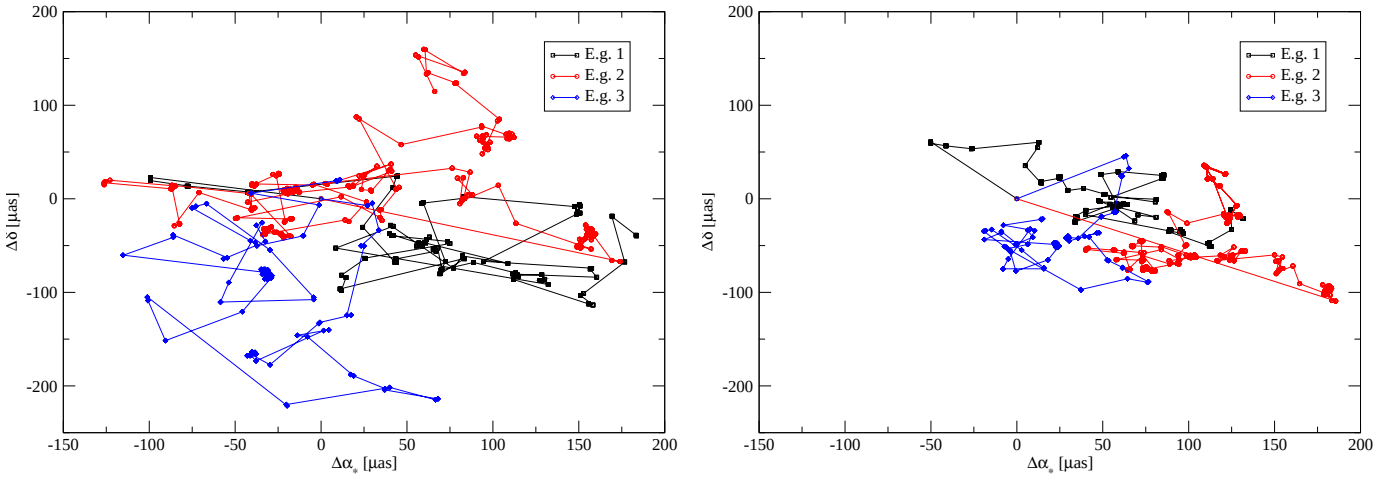

Fig. 2. Markov chain photocentre variability for a VLBI quasar with time scales, τ, of 2 years (left) and 10 years (right). In each case three examples are given for the same sources.

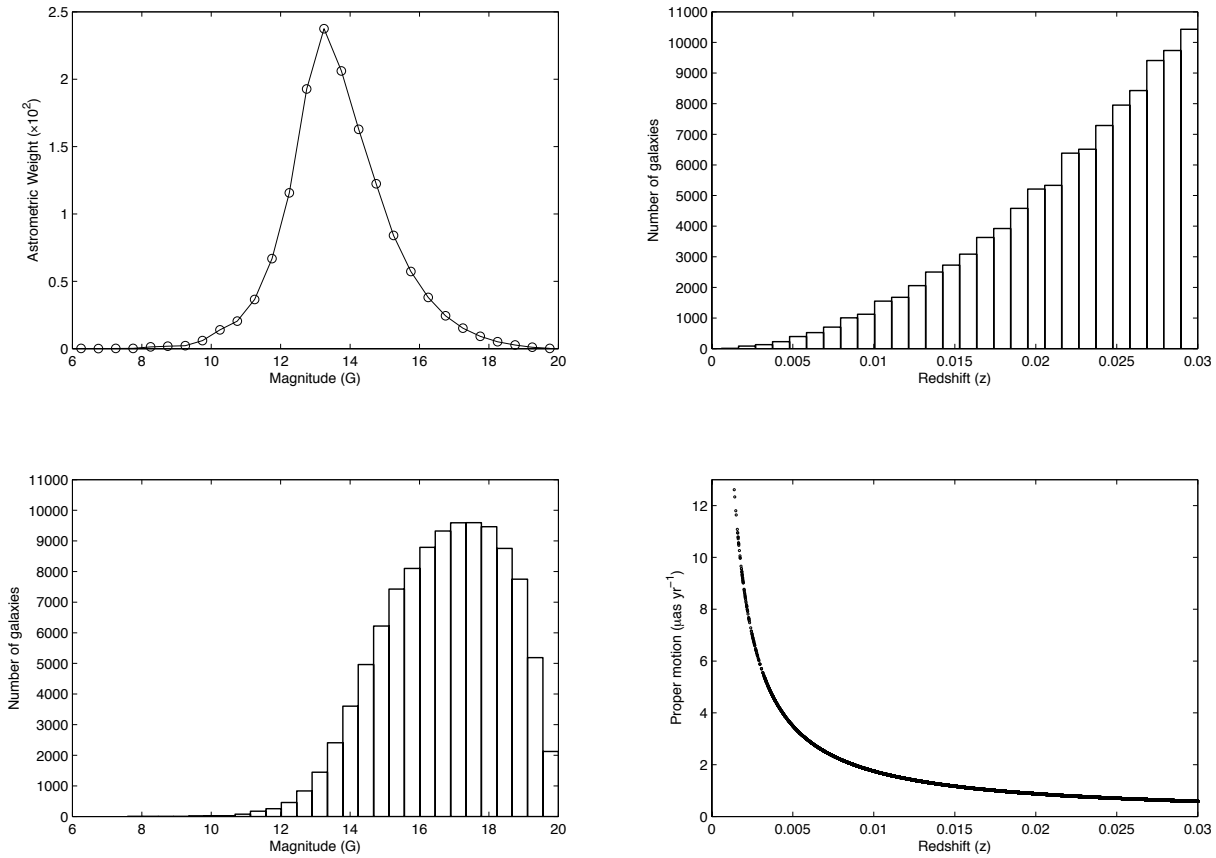

Fig. 3. Left: the astrometric weight (w) of GUMS galaxy observations (see **?**), where $w = \sum_{\rm obs} \sigma_{\rm obs}^{-2}$, is the total statistical weight of the assumed along-scan standard error of Gaia observations. Below is the number of GUMS galaxies as a function of G magnitude. Comparing the two left plots one can see that the largest astrometric weight is from $G = 12$ to $G = 16$ but the number of galaxies peaks around $G = 17$. Right: the distribution of the galaxies from GUMS and the magnitude of the cosmological proper motion effect as a function of redshift.

the reference frame we compare the final positions and proper motions with different realizations of their true values, assuming a random variation of 100 μas for VLBI_QUASARS in position and 10 μas yr^{-1} in proper motion for all quasars. For the simulations we use an antapex direction in galactic coordinates of ($l = 83.99°$, $b = -48.26°$). We assumed a Galactocentric acceleration of 4.3 μas yr^{-1}, CMB velocity of 369.0 km s^{-1}, a Hubble constant of 67.3 km s^{-1} Mpc^{-1} and a 5 year mission.

4. Determination of the reference frame and proper motion patterns

The relative measurement principle of Gaia results in astrometric parameters (positions and proper motions) which are determined with respect to six degrees of freedom in the orientation $\boldsymbol{\epsilon} = (\epsilon_x,\ \epsilon_y,\ \epsilon_z)$ and the spin $\boldsymbol{\omega} = (\omega_x,\ \omega_y,\ \omega_z)$ of the Gaia reference frame relative to the ICRS at an adopted frame rotator epoch, $t_{\rm fr}$, which need not be the same as the reference epoch of the astrometric parameters. To express the final astrometric results in a celestial reference frame which closely matches the ICRS, the $\boldsymbol{\epsilon}$ and $\boldsymbol{\omega}$ parameters must be estimated from several sets of sources in a least squares solution. The determined parameters can then be used to correct the reference frame to coincide with the ICRS. This frame rotation determination is made subsequent to the Astrometric Global Iterative Solution (AGIS; Lindegren et al. 2012) using three different sets of sources:

- VLBI_QUASAR (S_P) – a subset consisting of the optical counterparts of a few thousand radio VLBI objects with known positions and proper motions in the ICRS independent of Gaia, which help to constrain $\boldsymbol{\epsilon}$. They are typically the optical counterparts of extragalactic objects with accurate positions from VLBI. These quasars can also be used to calculate the spin parameter ($\boldsymbol{\omega}$), but being very small in number, their contribution to the determination of spin is small.
- GAIA_QUASAR (S_{NR}) – a larger subset consisting of hundreds of thousands of quasar-like objects ($\sim 10^5 - 10^6$) taken from ground based and photometric surveys which help to constrain $\boldsymbol{\omega}$. These quasars do not have accurately known positions in ICRS so cannot be used to calculate $\boldsymbol{\epsilon}$. They are assumed to define a kinematically non-rotating celestial frame.
- ICRS_STAR (S_{PM}) – a subset of primary sources that have positions and/or proper motions that are accurately determined with respect to the ICRS independent of Gaia. This could include radio stars observed by radio VLBI interferometry, or stars whose absolute proper motions have been determined by some other means.

For the present investigation we do not consider the subset ICRS_STAR set but add another subset of point like sources at low redshift ($z < 0.03$):

- GAIA_GALAXY – a subset of point like galactic nuclei sources with known redshift that may have measurable proper motion, albeit small. This subset can be used to probe redshift dependent proper motion patters (see Sect. 2.3).

The determination of the orientation and spin parameters together with the acceleration parameters, combined into a single parameter array $\boldsymbol{\theta} = [\epsilon_x\ \epsilon_y\ \epsilon_z\ \omega_x\ \omega_y\ \omega_z\ a_x\ a_y\ a_z]'$ is done using a least-squares estimation of the positions and proper motions of subsets GAIA_QUASAR and VLBI_QUASAR in the two frames. For GAIA_QUASAR the expression for the apparent proper motion in the Gaia reference frame is given by Eq. (108) in Lindegren et al. (2012), namely

$$\mu_{\alpha*} = \boldsymbol{q}'\boldsymbol{\omega} + \boldsymbol{p}'\boldsymbol{a} \tag{9}$$

$$\mu_{\delta} = -\boldsymbol{p}'\boldsymbol{\omega} + \boldsymbol{q}'\boldsymbol{a} \tag{10}$$

and the corresponding Eq. (110) for VLBI_QUASAR simplifies to

$$\Delta\alpha* = \boldsymbol{q}'\boldsymbol{\epsilon} \tag{11}$$

$$\Delta\delta = -\boldsymbol{p}'\boldsymbol{\epsilon} \tag{12}$$

if the position differences are measured at the reference epoch $t_{\rm ep}$. In these equations $\boldsymbol{p} = (-\sin\alpha,\ \cos\alpha,\ 0)$ and $\boldsymbol{q} = (-\sin\delta\cos\alpha,\ -\sin\delta\sin\alpha,\ \cos\delta)$.

Once the parameters $\boldsymbol{\epsilon}$, $\boldsymbol{\omega}$ and $\boldsymbol{a}$ have been determined, the GAIA_GALAXY subset of low red-shift galaxies can be used to estimate the redshift dependent parameters. To determine the velocity of the Solar System relative to the CMB we must assume we know the Hubble constant and we can then do a similar solution for $\boldsymbol{\theta} = [v_x\ v_y\ v_z\ a_x\ a_y\ a_z]'$, assuming $\boldsymbol{\epsilon}$, $\boldsymbol{\omega}$ and H_0 are known. Conversely, if we assume that the velocity of the Solar System relative to the CMB is known, then it is possible to determine H_0 by solving for $\boldsymbol{\theta} = [H_0\ a_x\ a_y\ a_z]'$. Note that it is not necessary to solve for the acceleration term in each case but the acceleration effect is also present when using low redshift galaxies and hence it is useful to include it as a consistency check and to obtain the correlation. For these secondary calculations[2], we cannot use the quasars as the effect falls off rapidly with increasing redshift and most quasars would contribute very little to the solution (see Sect. 3.3).

5. Results

To determine how well we recover the reference frame we run one hundred different realizations of the various simulation cases described below. The results of a comparison between the results and the true values gives the errors from which the mean and standard deviation values are found.

Table 2 gives a summary of the different simulations done. Case A is a reference data set where only Gaia nominal observation noise and the nominal attitude noise is added. Using the same noise assumptions cases B-C then assess the impact of adding quasar variability with different characteristic relaxation time scales. Finally, case D shows the results of using the IGQL (Véron-Cetty & Véron 2010; Souchay et al. 2012; Andrei et al. 2009; Shen et al. 2011; Pâris et al. 2014; Andrei et al. 2012) under nominal conditions similar to case A to determine the impact of using a non-uniform sky distribution.

In each of these cases, a first simulation is done using quasars to accurately determine the reference frame parameters, $\boldsymbol{\epsilon}$ and $\boldsymbol{\omega}$, and the acceleration of the Solar System, $\boldsymbol{a}$. Then in two independent secondary simulations we use the values of $\boldsymbol{\epsilon}$ and $\boldsymbol{\omega}$ found using the quasars to determine either the instantaneous velocity of the Solar System relative to the CMB, or the Hubble constant using low redshift galaxies as described in Sect. 4. As these parameters are degenerate we cannot solve for both at the same time and hence we have two secondary simulations. For the secondary galaxy simulations no variability is assumed and we also calculate the acceleration of the Solar System, $\boldsymbol{a}$, which is less accurate as we now use fewer sources. The assumption of using fewer sources may be pessimistic given that the number of objects detected by Gaia is much higher but a detailed study of the centroiding accuracy for galaxies is needed for a more realistic simulation of this effect.

Table 3 shows the results of the reference frame determination based on quasars for cases A-D. For the reference case A the mean value for Galactocentric acceleration, which is determined simultaneously with the reference frame, is $|\boldsymbol{a}| = 4.304\ \mu$as yr^{-1} with a standard deviation and mean formal error of $\sim 0.26\ \mu$as yr^{-1} compared to the simulated input value of

[2] In principle it would be possible to directly combine the primary with a secondary calculation but it practice the primary calculation is the baseline for the Gaia data processing and it was decided not to complicated this critical software.

Table 2. The table summarises the different simulations. In all cases the nominal Gaia observation noise and a nominal attitude noise of 10 μas is used. Case A is an ideal reference simulation while cases B and C introduce quasar variability with different relaxation time scales. In case D we use the IGQL dataset to show the impact of a non-uniform sky distribution. The CMB velocity induced proper motion pattern is towards the antapex direction in galactic coordinates of ($l = 83.99°$, $b = -48.26°$). We assumed a Galactocentric acceleration of 4.3 μas yr^{-1}, CMB velocity of 369.0 km s^{-1}, a Hubble constant of 67.3 km s^{-1} Mpc^{-1} and a 5 year mission.

Data Set	Case	Characteristic Time τ [yr]	VLBI_QUASAR $\sigma_{\text{var.}}[\mu\text{as}]$	GAIA_QUASAR $\sigma_{\text{var.}}[\mu\text{as}]$
Case A	GUMS	–	0	0
Case B	GUMS	2	100	100
Case C	GUMS	10	100	100
Case D	IGQL	–	0	0

Table 3. Results from simulations based on using the GUMS quasar dataset with a uniform sky distribution apart for the Galactic plane. Case A IGQL uses the IGQL quasar dataset with a non-uniform sky distribution particularly in the southern hemisphere (see Figure 4).

		Orientation ($\boldsymbol{\epsilon}$) [μas]			Spin ($\boldsymbol{\omega}$) [μas yr^{-1}]			Acceleration ($\boldsymbol{a}$) [μas yr^{-1}]		
		x	y	z	x	y	z	x	y	z
Case A	Mean	-0.249	-0.234	-0.126	0.001	-0.004	-0.003	4.304	0.003	-0.026
	Std	3.282	3.425	3.069	0.125	0.158	0.166	0.149	0.144	0.157
	$\langle\sigma\rangle$	2.211	2.254	2.445	0.144	0.147	0.159	0.145	0.146	0.159
Case B	Mean	0.169	0.182	0.428	-0.003	0.001	0.007	4.308	0.002	-0.007
	Std	3.909	3.695	4.329	0.145	0.182	0.167	0.162	0.152	0.175
	$\langle\sigma\rangle$	2.239	2.284	2.473	0.154	0.156	0.169	0.154	0.155	0.169
Case C	Mean	0.216	-0.072	-0.148	-0.014	0.013	0.016	4.307	0.009	-0.001
	Std	4.605	4.281	4.469	0.136	0.178	0.171	0.154	0.146	0.165
	$\langle\sigma\rangle$	2.260	2.304	2.494	0.148	0.150	0.163	0.148	0.150	0.163
Case D	Mean	3.818	0.633	1.427	-1.083	-4.473	1.184	5.578	1.657	-1.654
	Std	3.217	3.779	4.559	0.151	0.165	0.185	0.175	0.151	0.203
	$\langle\sigma\rangle$	2.157	2.136	2.838	0.171	0.167	0.211	0.172	0.167	0.211

4.3 μas yr^{-1}. This shows that under optimal conditions the Galactocentric acceleration can be well determined to a few percent and the mean values are consistent with the standard deviation and mean formal errors. The general trend is as expected when comparing cases A to D as each case adds additional complexity and the errors, standard deviation and the mean formal errors all increase slightly.

The addition of photocentre variability in cases B and C with characteristic time scales of 2 and 10 years respectively does not significantly degrade the solution for Galactocentric acceleration. The mean value for Galactocentric acceleration is very similar at $|\boldsymbol{a}| = 4.308$ μas yr^{-1} but both the standard deviation and the mean formal errors of these runs only increase very modestly and are in rough agreement with, but slightly better than, the predictions of Perryman et al. (2014). These differences can be partially explained by the use of different numbers of quasars in the two estimates – 170 000 in theirs and 500 000 in ours.

In addition to using the GUMS quasar data, which is well distributed on the sky apart from the Galactic plane, we have also used the IGQL dataset in case D. The results for acceleration are poorer (for the IGQL we get a value of $|\boldsymbol{a}| = 6.049$ μas yr^{-1} with significant components directed away from the galactic centre) but the standard deviations and formal errors do not change considerably from Case A. The reason for different mean value is the non-uniform sky distribution of the data set, particularly in the southern hemisphere where the data set is rather sparse (see Figure 4) compared to the GUMS catalogue. This results in the spin parameter ($\boldsymbol{\omega}$) being poorly determined for the reference frame and consequently this impacts the determination of the acceleration vector. By comparing the resulting correlation matrices for GUMS and IGQL one can see in Table 4, highlighted in red, that a weak correlation exists between the components of $\boldsymbol{\omega}$ and $\boldsymbol{a}$ in the GUMS catalogue but this is much stronger in the IGQL data set. The IGQL will be used in the early Gaia processing and care should be taken when interpreting the reference frame and Galactocentric acceleration results. However, as Gaia detects more quasars itself the sparse distribution found in the IGQL catalogue will be filled in and the results presented here based on the GUMS catalogue should become more representative. Note that many of the elements of the correlation matrix are zero, this results purely from our choice of reference frame epoch and the source reference epochs which are all the same. Choosing different reference times would result in non-zero entries in the correlation matrix but for comparison purposes the current choice is more useful.

In Table 5 the results from simulations using low redshift galaxies from the GUMS catalogue are presented. We firstly determine the individual reference frame parameters $\boldsymbol{\epsilon}$ and $\boldsymbol{\omega}$, us-

Table 4. The symmetric correlation matrix calculated from the frame rotation ($\boldsymbol{\epsilon}$, $\boldsymbol{\omega}$) and acceleration ($\boldsymbol{a}$) parameters for a GUMS dataset (upper right triangle) to be compared with an IGQL dataset (lower left triangle). Note the major differences in the IGQL results which are highlighted in red. There is a significantly stronger correlation between $\boldsymbol{\omega}$ and $\boldsymbol{a}$ which leads to poorer results.

	ϵ_x	ϵ_y	ϵ_z	ω_x	ω_y	ω_z	a_x	a_y	a_z
ϵ_x	**1.0**	0.001	-0.025	0.000	0.000	0.000	0.000	0.000	0.000
ϵ_y	0.038	**1.0**	0.017	0.000	0.000	0.000	0.000	0.000	0.000
ϵ_z	-0.037	-0.045	**1.0**	0.000	0.000	0.000	0.000	0.000	0.000
ω_x	0.000	0.000	0.000	**1.0**	0.003	-0.021	0.000	0.010	0.010
ω_y	0.000	0.000	0.000	0.106	**1.0**	0.011	-0.010	0.000	-0.048
ω_z	0.000	0.000	0.000	0.071	-0.182	**1.0**	-0.010	0.049	0.000
a_x	0.000	0.000	0.000	0.002	-0.444	0.328	**1.0**	0.011	-0.016
a_y	0.000	0.000	0.000	0.444	-0.004	0.264	0.118	**1.0**	0.001
a_z	0.000	0.000	0.000	-0.330	-0.262	0.002	0.078	-0.189	**1.0**

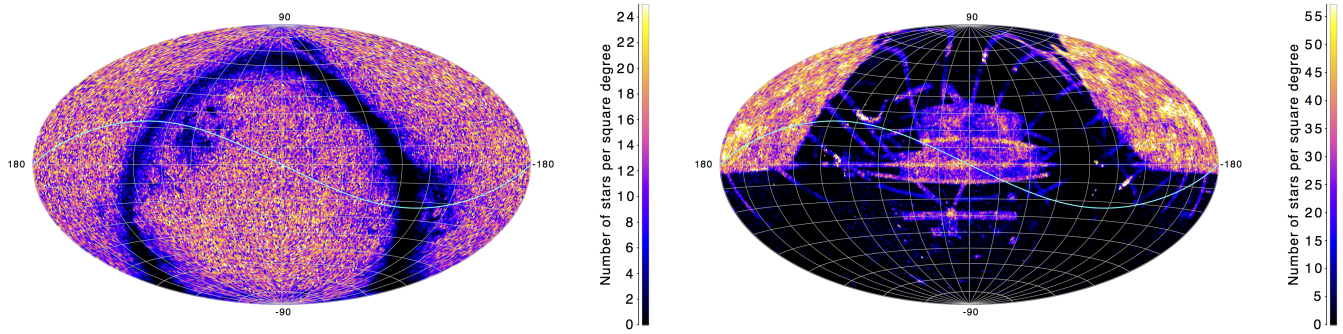

Fig. 4. All-sky maps showing the median number of sources per pixel in an equatorial Hammer-Aitoff projection. *Left:* The quasar distribution on the sky from the GUMS catalogue. *Right:* The quasar distribution on the sky from the IGQL catalogue. The cyan line denotes the ecliptic.

Table 5. Results from simulations using the GUMS galaxy catalogue for all cases. Note that the quasars are firstly used to determine the reference frame parameters $\boldsymbol{\epsilon}$ and $\boldsymbol{\omega}$ which are then fixed. Then in two independent secondary simulations based on low redshift galaxies we determine in the first case the Galactocentric acceleration together with the instantaneous velocity of the Solar System with respect to the CMB and in the second case the Galactocentric acceleration together with the Hubble constant. The two estimates of the acceleration based on galaxies gave very similar results (to within a few percent) so only those from the first case are tabulated.

		Acceleration ($\boldsymbol{a}$) [μas yr^{-1}]			Velocity ($\boldsymbol{v}$) [km s^{-1}]				Direction [°]		Hubble constant [km s^{-1} Mpc^{-1}]
		x	y	z	x	y	z	$\lvert\boldsymbol{v}\rvert$	l	b	H_0
Case A	Mean	4.342	0.029	-0.005	20.053	234.445	-273.981	361.154	85.111	-49.343	65.748
	Std	0.241	0.195	0.234	65.904	55.394	64.385	107.505			11.722
	$\langle\sigma\rangle$	0.270	0.269	0.270	98.403	97.522	96.899	169.066			18.034
Case B	Mean	4.300	0.016	-0.017	27.487	238.212	-270.408	361.415	83.417	-48.434	65.895
	Std	0.214	0.217	0.211	53.767	56.126	61.535	99.134			10.991
	$\langle\sigma\rangle$	0.271	0.270	0.270	98.665	97.796	97.166	169.529			18.153
Case C	Mean	4.299	0.016	-0.018	27.524	238.205	-270.348	361.369	83.409	-48.428	65.887
	Std	0.214	0.217	0.211	53.758	56.108	61.481	99.086			10.984
	$\langle\sigma\rangle$	0.271	0.270	0.270	98.665	97.796	97.166	169.529			18.153
Case D	Mean	4.328	0.045	0.194	17.152	238.202	-299.719	383.231	85.881	-51.452	69.711
	Std	0.219	0.221	0.208	60.978	55.090	57.167	100.106			11.190
	$\langle\sigma\rangle$	0.275	0.274	0.275	100.173	99.303	98.691	172.150			18.053

ing the quasar simulations tabulated in Table 3, which are then fixed input for theses secondary simulations. Two independent secondary simulations are done. Firstly we determine the instantaneous velocity of the Solar System with respect to the CMB together with the acceleration. Secondly, the Hubble constant together with the acceleration. It is not necessary to make these two estimates of the acceleration based on low redshift galaxies but doing so allows the correlation with the parameters of interest to be estimated and it provides a consistency check with the value determined from the quasar data.

If we compare the results for the acceleration determined from the low redshift galaxies with that determined from the

quasars in Table 3, we see that the actual values do not change significantly. However, the standard deviation and mean formal errors have increased by factors of ∼1.5 and ∼1.8 respectively, for Case A, which is slightly less that the expected value of $\sqrt{5}$ due to the difference in the number of objects used. This discrepancy is probably due the lack of variability in the galaxy observations and that the galaxies are slightly brighter than the quasars (the number of galaxies peaks at ∼17 G magnitude – see Figure 3 bottom left). Little information on the centroiding accuracy of point like galaxies (or components thereof) is presently available and our current values certainly underestimate the real errors. The differences of the acceleration determined from the two secondary simulations are well within the expected variance and thus we have only reported those from the velocity case. In addition, for case D, the acceleration results are actually much better. This is because case D in Table 3 used the IGQL quasar dataset, with a non-uniform sky distibution, to estimate the values of $\boldsymbol{\epsilon}$, $\boldsymbol{\omega}$ and $\boldsymbol{a}$ while in Table 5 we use the uniformally distributed galaxies to estimate the acceleration which now gives better results. Clearly the sky distribution is important.

The results for the instantaneous velocity of the Solar System with respect to the CMB are also tabulated in table 5. The recovered components of the velocity, magnitude and direction are given. In the simulations we use an apex direction of ($l = 263.99°$, $b = 48.26°$) and a magnitude of $|\boldsymbol{v}| = 369$ km s^{-1}. The recovered mean values and direction are in good agreement (within five percent) in all simulations. The magnitude of the standard deviation is just over 100 km s^{-1} while the magnitude of the mean formal error is of the order of 170 km s^{-1}. These errors are relatively large but one must remember we have used only 100 000 objects in the redshift range $z < 0.03$ while the largest contribution to this effect is dominated by a small number of objects in the range $z < 0.01$ (see Figure 3 right). The results given in Table 5 for case D are slightly worse as the fixed reference frame parameters $\boldsymbol{\epsilon}$ and $\boldsymbol{\omega}$ were less accurately determined using the IGQL quasars and thus they also have a small impact the determination of the proper motion patterns in these secondary simulations.

Likewise for the Hubble constant the recovered mean values are in good agreement (within four percent) in all simulations. Again the errors are relatively large, the standard deviation is 11-12 km s^{-1} Mpc^{-1} while the mean formal error is of the order of 18 km s^{-1} Mpc^{-1}. Clearly, detecting more sources in the low redshift range $z < 0.01$ would greatly improve these results but it remains unclear for now how many more objects could be used for this determination and how well such extended objects can be centroided.

6. Conclusions

In this paper we have assessed how well Gaia can improve the ICRF using sets of quasars to define a kinematically stable non-rotating reference frame with the barycentre of the Solar System as its origin. Photocentric variability of the quasars has been simulated using a Markov chain model at the level of 100 μas and does not appear to significantly perturb the results for either the reference frame determination or the proper motion pattern due to the acceleration of the solar system.

The IGQL does not have an ideal sky distribution to determine the reference frame or proper motion patterns and care should be taken in early Gaia data processing when interpreting theses results. However as Gaia detects more quasars itself the sky distribution will improve and eventually become more uniform and representative of the GUMS catalogue used in these simulations.

In this paper we have reviewed the various proper motion effects that could have an impact on the Gaia data processing and we have tried to quantify their respective magnitudes. Most of the effects are either not detectable by astrometry or do not seem to be strong enough to be reliably detected by Gaia. However, a cosmological proper motion pattern due to the instantaneous velocity of the Solar System with respect to the CMB might be just about measurable. In contrast to the acceleration of the Solar System this Cosmological proper motion pattern is redshift dependent and only significant at low redshift. Thus it cannot be determined from the more distant quasars and instead low redshift point like galaxies must be used. This source type has not yet been considered in the baseline processing for the Gaia mission.

From this proper motion pattern our velocity relative to the CMB can be determined provided we assume the Hubble constant is known. Likewise, if we assume our velocity is know from other missions, such as Planck, we can estimate the Hubble constant from this pattern of proper motions. We find that both measurements might be just within the reach of Gaia provided that a suitable set of low redshift point like objects can be identified and used in the processing. The onboard detection and data processing (centroiding) of such low redshift point like objects will ultimately limit whether this effect can be measured in practice.

Acknowledgements. The authors would like to thank the Swedish National Space Board (SNSB) for financial support without which this project would not have been possible.

Appendix A: Tables of local group and supercluster members.

Table A.1. The table below shows the values of proper motion, $\tilde{a}$, due to the extragalactic acceleration of various local group galaxies and some clusters of local supercluster.

Galaxy	M ($M_\odot$)	d (kpc)	$\tilde{a}$ (μas yr^{-1})
LMC	2.0×10^{10}	50	2.4×10^{-2}
M31	4.0×10^{11}	760	2.1×10^{-3}
Sagittarius	1.5×10^{08}	24	7.6×10^{-4}
SMC	8.0×10^{08}	59	7.0×10^{-4}
M33	1.4×10^{10}	830	6.1×10^{-5}
NGC6822	1.9×10^{09}	500	2.3×10^{-5}
UrsaMinor	1.7×10^{07}	63	1.3×10^{-5}
Cluster			
Virgo	1.2×10^{15}	16036	1.4×10^{-2}
Fornax	4.0×10^{13}	20491	2.9×10^{-4}
Norma	1.0×10^{15}	69937	6.2×10^{-4}
Antlia	3.3×10^{14}	41561	5.8×10^{-4}
Coma	7.0×10^{14}	102900	2.0×10^{-4}

The masses and the distances of galaxies have been taken from Van den Bergh et al. (2000). The distance of clusters are calculated from redshift data available at NED[3] and the masses are taken from (Fouqué et al. 2001; Nasonova et al. 2011; Boehringer et al. 1996; Hopp & Materne 1985; Gavazzi et al. 2009).

[3] Nasa Extragalactic Database: `http://ned.ipac.caltech.edu/`

Appendix B: Relation between proper motion of image and lens

Consider a point source Q and a lensing object L at a distance D_Q and D_L respectively from an observer O (see Fig. B.1). Let $\angle QOL = \alpha$ and $\angle Q'OL = \beta$, where Q' is the shifted image of source Q due to the presence of the lens. Then the lens equation is given by

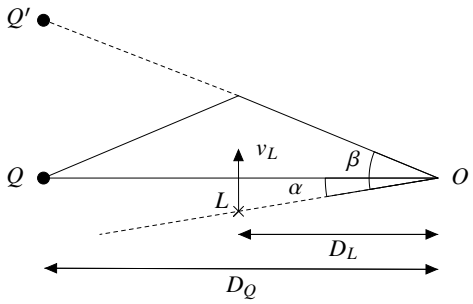

Fig. B.1. Lensing parameters.

$$\beta(\beta - \alpha) = \theta_E^2 = \frac{4GM_L}{c^2}\left(\frac{1}{D_L} - \frac{1}{D_Q}\right), \tag{B.1}$$

where θ_E is called the 'Einstein radius'. Let us assume that the point source is a quasar so that we can assume it to be at rest. Then the proper motion,

$$\mu_Q = 0$$

If the lens has a small velocity v_L along the direction perpendicular to the line of sight then the proper motion of lens is given by

$$\mu_L = \frac{v_L}{D_L} = -\frac{d\alpha}{dt}$$

The negative sign is chosen so that the lens motion and the image shift Q' are in the same direction. If the lens is moving then the image Q' will also be moving resulting in a proper motion

$$\mu_{Q'} = \frac{d(\beta - \alpha)}{dt} = \frac{d\beta}{dt} - \frac{d\alpha}{dt} = \frac{d\beta}{dt} + \mu_L$$

From Eq. (B.1)

$$\beta^2 - \beta\alpha - \theta_E^2 = 0\,.$$

The roots of this equation are given by

$$\beta = \frac{\alpha}{2} \pm \sqrt{\frac{\alpha^2}{4} + \theta_E^2}$$

and differentiating with respect to time gives

$$\frac{d\beta}{dt} = \frac{d\alpha}{dt}\left[\frac{1}{2} \pm \frac{1}{2}\left(1 + \frac{4\theta_E^2}{\alpha^2}\right)^{-1/2}\right].$$

Assuming that $\alpha \gg \theta_E$, and taking the positive sign for an image in one direction only, we get

$$\mu_{Q'} \approx 2\mu_L\left(\frac{\theta_E}{\alpha}\right)^2. \tag{B.2}$$

If we now consider a large number of lenses, L_1, L_2, L_2, ... with random proper motions μ_1, μ_2, μ_3, ... at angles, α_1, α_2, α_3, ... respectively, and assume for simplicity that they all have the same Einstein's radius θ_E, then the mean-square from Eq. (B.2) is

$$\left\langle \mu_Q'^2 \right\rangle = 4\left\langle \mu_L^2 \right\rangle \left\langle \left(\frac{\theta_E}{\alpha}\right)^4 \right\rangle$$

With Q as centre and α as radius, let us draw a spherical shell of thickness $d\alpha$ and let N be the number density of lenses. Then the thin spherical shell will contain $2\pi\alpha d\alpha N$ lenses and the expectation value of α^{-4} is given by

$$E\left(\alpha^{-4}\right) = \int_{\theta_E}^{\infty} 2\pi\alpha N \frac{1}{\alpha^4}\, d\alpha = \pi\theta_E^{-2} N$$

Therefore,

$$\left\langle \mu_Q'^2 \right\rangle = 4\left\langle \mu_L^2 \right\rangle \pi\theta_E^2 N$$

Here,

$$\tau \equiv \pi\theta_E^2 N$$

is the probability that Q will be inside Einstein ring of some lens which is also known as the 'optical depth'. So, we can finally arrive at

$$(\mu_{Q'})_{\rm RMS} = (\mu_L)_{\rm RMS} \times 2\sqrt{\tau} \tag{B.3}$$

References

Andrei, A. H., Anton, S., Barache, C., et al. 2012, in SF2A-2012: Proceedings of the Annual meeting of the French Society of Astronomy and Astrophysics, ed. S. Boissier, P. de Laverny, N. Nardetto, R. Samadi, D. Valls-Gabaud, & H. Wozniak, 61–66

Andrei, A. H., Souchay, J., Zacharias, N., et al. 2009, A&A, 505, 385

Bailer-Jones, C. A. L., Smith, K. W., Tiede, C., Sordo, R., & Vallenari, A. 2008, MNRAS, 391, 1838

Bastian, U. 1995, in ESA Special Publication, Vol. 379, Future Possibilities for bstrometry in Space, ed. M. A. C. Perryman & F. van Leeuwen, 99

Belokurov, V. A. & Evans, N. W. 2002, MNRAS, 331, 649

Boehringer, H., Neumann, D. M., Schindler, S., & Kraan-Korteweg, R. C. 1996, ApJ, 467, 168

Bombrun, A., Lindegren, L., Hobbs, D., et al. 2012, A&A, 538, A77

Book, L. G. & Flanagan, É. É. 2011, Phys. Rev. D, 83, 024024

Chatfield, C. 2013, The Analysis of Time Series: An Introduction, Sixth Edition, Chapman & Hall/CRC Texts in Statistical Science (Taylor & Francis)

Doob, J. L. 1942, Annals of Mathematics, 43, 351

ESA, ed. 1997, ESA Special Publication, Vol. 1200, The HIPPARCOS and TYCHO catalogues. Astrometric and photometric star catalogues derived from the ESA HIPPARCOS Space Astrometry Mission

Feng, F. & Bailer-Jones, C. A. L. 2013, ApJ, 768, 152

Fouqué, P., Solanes, J. M., Sanchis, T., & Balkowski, C. 2001, A&A, 375, 770

Gavazzi, R., Adami, C., Durret, F., et al. 2009, A&A, 498, L33

Ghez, A. M., Salim, S., Weinberg, N. N., et al. 2008, ApJ, 689, 1044

Gwinn, C. R., Eubanks, T. M., Pyne, T., Birkinshaw, M., & Matsakis, D. N. 1997, ApJ, 485, 87

Hinshaw, G., Weiland, J. L., Hill, R. S., et al. 2009, ApJS, 180, 225

Hobson, M. P., Efstathiou, G. P., & Lasenby, A. N. 2006, General Relativity (Cambridge University Press)

Hogg, D. W. 1999, ArXiv Astrophysics e-prints [astro-ph/9905116]

Holl, B., Lindegren, L., & Hobbs, D. 2012, A&A, 543, A15

Hopp, U. & Materne, J. 1985, A&AS, 61, 93

Kardashev, N. S. 1986, AZh, 63, 845

Klioner, S. A. 2003, AJ, 125, 1580

Klioner, S. A. 2004, Phys. Rev. D, 69, 124001

Kopeikin, S. M. & Makarov, V. V. 2006, AJ, 131, 1471

Kovalev, Y. Y., Lobanov, A. P., Pushkarev, A. B., & Zensus, J. A. 2008, A&A, 483, 759

Kovalevsky, J. 2003, A&A, 404, 743

Kristian, J. & Sachs, R. K. 1966, ApJ, 143, 379
Lewis, G. F. & Ibata, R. A. 1998, ApJ, 501, 478
Lindegren, L., Lammers, U., Hobbs, D., et al. 2012, A&A, 538, A78
Ma, C., Arias, E. F., Bianco, G., et al. 2009, IERS Technical Note, 35, 1
Ma, C., Arias, E. F., Eubanks, T. M., et al. 1998, AJ, 116, 516
MacMillan, D. S. 2005, in Astronomical Society of the Pacific Conference Series, Vol. 340, Future Directions in High Resolution Astronomy, ed. J. Romney & M. Reid, 477
Mignard, F. 2011, in Proceedings of the "Journées 2011 Systémes de référence spatio-temporels", eds.: Schuh, H., Böhm S., Nilsson T. and Capitaine N.
Nasonova, O. G., de Freitas Pacheco, J. A., & Karachentsev, I. D. 2011, A&A, 532, A104
Pâris, I., Petitjean, P., Aubourg, É., et al. 2014, A&A, 563, A54
Pasquato, E., Pourbaix, D., & Jorissen, A. 2011, A&A, 532, A13
Perryman, M., Spergel, D. N., & Lindegren, L. 2014, ApJ, 789, 166
Planck Collaboration, Aghanim, N., Armitage-Caplan, C., et al. 2014, A&A, 571, A27
Popović, L. Č., Jovanović, P., Stalevski, M., et al. 2012, A&A, 538, A107
Porcas, R. W. 2009, A&A, 505, L1
Pyne, T., Gwinn, C. R., Birkinshaw, M., Eubanks, T. M., & Matsakis, D. N. 1996, ApJ, 465, 566
Quercellini, C., Amendola, L., Balbi, A., Cabella, P., & Quartin, M. 2012, Phys. Rep., 521, 95
Quercellini, C., Cabella, P., Amendola, L., Quartin, M., & Balbi, A. 2009, Phys. Rev. D, 80, 063527
Robin, A. C., Luri, X., Reylé, C., et al. 2012, A&A, 543, A100
Sazhin, M. V., Sazhina, O. S., & Pshirkov, M. S. 2011, Astronomy Reports, 55, 954
Shen, Y., Richards, G. T., Strauss, M. A., et al. 2011, ApJS, 194, 45
Smith, A. G., Nair, A. D., Leacock, R. J., & Clements, S. D. 1993, AJ, 105, 437
Souchay, J., Andrei, A. H., Barache, C., et al. 2012, A&A, 537, A99
Sovers, O. J., Fanselow, J. L., & Jacobs, C. S. 1998, Reviews of Modern Physics, 70, 1393
Sparke, L. S. & Gallagher, III, J. S. 2000, Galaxies in the universe : an introduction
Taris, F., Souchay, J., Andrei, A. H., et al. 2011, A&A, 526, A25
Titov, O. 2009, in 19th European VLBI for Geodesy and Astrometry Working Meeting, ed. G. Bourda, P. Charlot, & A. Collioud, 14–18
Titov, O. 2010, in Sixth International VLBI Service for Geodesy and Astronomy. Proceedings from the 2010 General Meeting, "VLBI2010: From Vision to Reality". Held 7-13 February, 2010 in Hobart, Tasmania, Australia. Edited by D. Behrend and K.D. Baver. NASA/CP 2010-215864., p.60-64, ed. R. Navarro, S. Rogstad, C. E. Goodhart, E. Sigman, M. Soriano, D. Wang, L. A. White, & C. S. Jacobs, 60–64
Titov, O., Lambert, S. B., & Gontier, A.-M. 2011, A&A, 529, A91
Van den Bergh, S., King, A., Lin, D., et al. 2000, Galaxies of the Local Group (Cambridge: Cambridge Univ. Press)
Véron-Cetty, M.-P. & Véron, P. 2010, A&A, 518, A10
Weinberg, S. 2008, Cosmology (Oxford University Press)